Selectively lighting-up dimeric G-quadruplex forming aptamers with a thiazole orange derivative for efficient $VEGF_{165}$ targeting

Ettore Napolitano,[a] Claudia Riccardi,[a] Rosa Gaglione,[a] Angela Arciello,[a] Valentina Pirota,[b] Alice Triveri,[b] Filippo Doria,[b] Domenica Musumeci[a] and Daniela Montesarchio[a,*]

[a]*Department of Chemical Sciences, University of Naples Federico II, 80126 Naples, Italy*
[b]*Department of Chemistry, University of Pavia, 27100 Pavia, Italy*

Abstract
In order to develop efficient anticancer theranostic systems, we focused on the interaction between an easily prepared cyanine dye, analogue of thiazole orange (here named CyOH), and two G-quadruplex-forming aptamers, V7t1 and 3R02, that specifically recognize the Vascular Endothelial Growth Factor 165 ($VEGF_{165}$) − a critical angiogenic protein overexpressed in a variety of cancer cells, responsible for the rapid growth and metastases of solid tumors. We here demonstrated, by exploiting different biophysical techniques − i.e. circular dichroism (CD), UV-vis, and fluorescence spectroscopy, along with gel electrophoresis − that this cyanine probe interacted with both aptamers giving a marked fluorescence light-up only when bound to their dimeric forms. Interestingly, both oligonucleotides recognized $VEGF_{165}$ with higher affinity when adopting dimeric G-quadruplex forms, which are indeed largely prevalent over their monomeric forms in pseudo-physiological conditions. Notably, the fluorescence light-up produced by the probe was maintained also when the complexes between CyOH and the dimeric aptamers bound to the target protein, evidencing potential applications in diagnostics. The CyOH-aptamer complexes, tested on MCF-7 cancer cells using non-tumorigenic MCF-10 cells as a control, were effectively internalized in cells and colocalized with a fluorescently-labelled anti-VEGF-A antibody, allowing both recognition and detection of the target protein. Our experiments showed that the studied systems are promising tools for anticancer theranostic strategies, combining the therapeutic potential of the G4-forming anti-VEGF aptamers with the diagnostic efficacy of the selective fluorescence light-up cyanine probe.

Introduction
VEGF-A (Vascular Endothelium Growth Factor – type A) is a glycoprotein that includes many isoforms, and the main member of a cytokine family playing essential roles in angiogenesis, lymphangiogenesis, and vasculogenesis, thus favouring the growth of solid tumours and being involved in the onset and progression of most tumours and/or inflammations (1). This growth factor is recognized as a valid tumour biomarker and therapeutic target. Therefore, selectively targeting VEGF-A, and particularly its main isoforms $VEGF_{165}$ and $VEGF_{121}$ (2–4), can be an extremely important strategy for early detection and therapy of cancer in the context of precision medicine.
Several G-quadruplex(G4)-forming aptamers have been identified for the selective inhibition of VEGF-A (5). In detail, Nonaka *et al.* selected the aptamer V7t1, which exhibited high affinity for both $VEGF_{165}$ (K_d = 1.4 nM) and $VEGF_{121}$ (K_d = 1.1 nM) (6). An *in silico* maturation, as post-SELEX (Systematic Evolution of Ligands by EXponential Enrichment) optimization of this aptamer, allowed obtaining four novel aptamers, the best of which was 3R02, showing an improved affinity for $VEGF_{165}$ with respect to V7t1 (K_d = 0.3 nM) (7).
In our previous studies, we demonstrated that V7t1, in the presence of physiological extracellular Na^+ concentrations, has a very different conformational behaviour if subjected or not to annealing procedures. Indeed, not-annealed V7t1 (N.A. V7t1) mainly forms dimeric parallel G4 structures, while the annealed oligonucleotide (A. V7t1) adopts a monomeric antiparallel G4 folding. Remarkably, only the dimeric aptamer efficiently binds $VEGF_{165}$, showing a higher affinity for the protein compared to the monomeric species, as determined by electrophoresis mobility shift assay (EMSA) experiments (8). These results were explained in terms of multivalency effects which can be operative in dimeric or multimeric forms of aptamers, conferring them higher binding affinity in target recognition (9, 10).
If detailed studies have been carried out to disclose the conformational behaviour of V7t1 and particularly of some well-structured V7t1 analogues (11), not much is known about 3R02, whose reported CD spectra are indicative of a highly polymorphic G4-forming oligonucleotide (7).
We reasoned that the specific and high-affinity VEGF-binders V7t1 and 3R02 could produce efficient tools for VEGF targeting if associated with finely tunable, conformation-sensitive detection systems. Probes with a high affinity for these aptamers – in principle selectively binding and stabilizing the oligonucleotides in their bioactive conformations or in the most bioactive ones – forming with them stable complexes still recognized by the protein, would be particularly attractive to our purposes. In this frame, G4-forming aptamers equipped with suitable fluorescence probes, sensitive to the G4 folding/unfolding processes, offer very promising systems for *in vitro* and *in vivo* applications. Indeed, several fluorescent ligands have been designed for the detection of G4 structures (12–14). Among the known selective and high-affinity binders of G4 structures, cyanine dyes play a prominent role (15–18),

offering several advantages as versatile molecules, easy to synthesize and *ad hoc* functionalize, allowing a fine-tuning of their G4 binding affinity and optical properties (15, 17, 18).
Thiazole orange (TO, 4-[3-methyl-2,3-dihydro(benzo-1,3-thiazole)-2-methylidene]quinolinium iodide), one of the most representative dyes of this class, is characterized by a very low intrinsic fluorescence in aq. solutions, marked chemical stability and high molar absorption coefficient. It can interact with different structures of DNA and RNA, showing a remarkable fluorescence turn-on response (19). When TO interacts with G-quadruplex structures, a fluorescence enhancement more than 2-fold higher than with duplexes is observed (20). This behaviour is strictly connected with the intramolecular rotation around the C-C bond connecting the benzothiazole and quinoline heterocycles which compose the TO structure: when these moieties are free to rotate around this bond, for example when the ligand is dissolved alone in aq. solutions, its fluorescence is almost null. Upon interaction with duplex DNA, the molecular target acts as a rigid cage forcing TO into a fully planar conformation, which can thus form stable intercalation complexes between adjacent Watson-Crick base pairs. With G4 structures, TO can bind the terminal G-quartets which offer a larger aromatic surface compared to base pairs of duplex structures, thus allowing more intense π-π stacking interactions and higher fluorescence response of the ligand (21).
Considering the intriguing properties of TO, we focused our attention on TO analogues as potential binders of the anti-VEGF G4-forming aptamers V7t1 and 3R02. In particular, we selected a TO derivative, here named CyOH (Scheme 1) (22–31), designed to provide better solubility in aq. solutions and a lower tendency to self-aggregate compared to the parent ligand but still maintaining the G4 recognition ability typical of TO. We thus analysed the interaction of CyOH with the G4-forming aptamers V7t1 and 3R02 by different biophysical techniques, determining the stability and properties of the resulting complexes. We particularly investigated the fluorescence response of CyOH when bound to either V7t1 or 3R02 in relation to the aptamer conformation, molecularity, and specific recognition by the protein. Finally, we evaluated the antiproliferative activity of the CyOH-aptamer complexes on MCF-7 breast cancer cells, using non-cancer MCF-10 cells as a control, by MTT assays, as well as their cell uptake and colocalization with a fluorescently-labelled VEGF-specific antibody by confocal laser scanning microscopy (CLSM) analysis.

Experimental Section

V7t1-VEGF$_{165}$ chemiluminescence-based binding studies

In this assay 100 µL of 0.2 µM VEGF$_{165}$-His solution in phosphate-buffered saline (PBS: 137 mM NaCl, 2.7 mM KCl, 8.1 mM NaH_2PO4/Na_2HPO_4, 1.86 mM KH_2PO_4/K_2HPO_4) were added to a copper-coated 96-well plate (Copper Coated High-Capacity Plates, Thermo Scientific) and incubated under gentle shaking for 1 h. Then, the supernatant was removed and each well was washed three times using 200 µL of a HEPES/Na^+ solution containing 0.05% (v/v) Tween-20 (Sigma-Aldrich). After washing, 100 µL of various concentrations of either N.A. or A. V7t1-biotin in HEPES/Na^+ were added to the wells and incubated for 1 h. In detail, 2.5, 5.0, 10, 12.5, 15, 20, 30, and 50 pmol of N.A. or A. V7t1-biotin in HEPES/Na^+ were added to each well. The wells were washed in the same conditions and then streptavidin-HRP (Horseradish peroxidase, BPS Bioscience) in Blocking Buffer (HEPES-Na^+ with 0.05% (v/v) Tween 20 and 2% (m/v) BSA) was added to each well and incubated under gentle shaking for 1 h. After three washes, enhanced chemiluminescence (ECL) HRP substrate (BPS Bioscience) was added and the HRP activity was measured by a multilabel plate counter (Glomax Discover System, GM3000). All experimental procedures were performed at r.t. in duplicate. The data were then reported in a graph as a function of DNA concentration. The obtained points were then fitted with an independent and equivalent-sites model (32), using the Origin 8.0 program, with the following equation:

$$\alpha = \left(\frac{1}{2[L]_0}\right)\left\{\left([L]_0 + n[Qu] + \frac{1}{K_b}\right) - \sqrt{\left([L]_0 + n[Qu] + \frac{1}{K_b}\right)^2 - 4[L]_0 n[Qu]}\right\}$$

where α is the mole fraction of ligand in the bound form, $[L]_0$ is the total ligand concentration, $[Qu]$ is the added DNA concentration, n is the number of the equivalent and independent sites on the DNA structure and K_b is the binding constant. The fraction of the bound ligand was determined by using the following equation:

$$\alpha = \frac{Y - Y_0}{Y_b - Y_0}$$

where Y, Y_0, and Y_b are the values of fluorescence emission intensity at the maximum, respectively, at each titrant concentration, at the initial and final state of the titration. The errors associated with the binding constant values are based on the fit.

General methods for the synthesis of CyOH

Solvents and reactants for the synthesis of CyOH were purchased from TCI or Merck and used as supplied without further purification. Thin-layer chromatography (TLC) analyses were carried out on silica gel plates (Merck 60F-254) with visualization at 254 and 366 nm. HPLC analyses were performed using an Agilent system SERIES 1260 with

XBridge® BEH C18 column (2.5 µm, 4.6 x 50 mm) with a flow rate of 1.4 mL/min. HPLC purifications were carried out on an Agilent Technologies 1260 Infinity preparative HPLC provided with a diode array UV-vis detector, using a Waters XSelect CSH Phenyl-Hexyl column (5 µm, 150 x 30 mm) with a flow rate of 27 mL/min. For HPLC analyses and purifications, an aq. solution containing 0.1% TFA (trifluoroacetic acid) and acetonitrile were used as solvents A and B, respectively. The following methods were used: i) Method 1: first isocratic elution over 17 min with 95% solvent A/5% solvent B, then linear gradient to 60% solvent A/40% solvent B in 3 min, followed by isocratic elution for 2 min and then back to 95% solvent A/5% solvent B for 4 min (λ detection: 230, 256 and 300 nm); ii) Method 2: first isocratic elution over 2 min with 95% solvent A/5% solvent B, then linear gradient to 60% solvent A/40% solvent B in 14 min, followed by a linear gradient to 40% solvent A/60% solvent B in 8 min, and then 95% solvent A/5% solvent B isocratic elution for 1 min (λ detection: 256, 300 and 500 nm). ^{1}H- and ^{13}C-NMR spectra were recorded on Bruker Avance 300 MHz. All the chemical shifts (δ) are expressed in ppm with respect to the residual solvent signal for ^{1}H-NMR spectra. UPLC-ESI-MS data were recorded using a surveyor UPLC system equipped with a BEH Acquity UPLC column (1.7 µm, 2.1 x 50 mm), and an LCQ ADV MAX ion-trap mass spectrometer, with an electrospray ionization (ESI) source.

Synthesis of 1-(3-hydroxypropyl)-4-methylquinolinium iodide (2)

A mixture of 4-methylquinoline **1** (1 eq, 100 mg, 84 µL, 0.70 mmol) and 3-iodo-1-propanol (2.5 eq, 325 mg, 168 µL, 1.75 mmol) in 700 µL ethanol was refluxed for 72 h. After cooling to r.t. the mixture was treated with the minimum amount of methanol and then diethyl ether was added to allow precipitation of the target compound as a white solid. The precipitate was collected, washed three times with diethyl ether, and purified by preparative HPLC using isocratic elution with a 95:5 CH_3CN:H_2O/0.1% TFA solution over 24 min. All the HPLC fractions containing the compound of interest were collected and taken to dryness, affording desired product **2** with a 90% yield. A comparison of NMR data with those available in the literature confirmed the identity and purity of the obtained compound (33). **^{1}H-NMR** (300 MHz, CD_3OD): δ (ppm) 2.27 (q, 2H), 3.07 (s, 3H), 3.68 (t, 2H), 5.15 (t, 2H), 7.95 – 8.10 (m, 2H), 8.18 – 8.21 (m, 1H), 8.23 – 8.31 (m, 2H), 9.23 (d, 1H). **UPLC-ESI-MS** (positive mode) m/z: 202.3 (**2** + 1H$^+$)$^+$ a.m.u.

Synthesis of 3-methyl-2-(methylthio)benzo[d]thiazol-3-ium iodide (4)

Commercially available 2-(methylthio)benzo[d]thiazole **3** (1 eq, 70 mg, 0.39 mmol) was dissolved in methyl iodide (30 eq, 730 µL, 11.6 mmol) at r.t. The reaction mixture was refluxed at 100 °C for 15 h. A white precipitate was obtained, filtered, and repeatedly washed with diethyl ether to give product **4** with a 92% yield. A comparison of the experimental with literature data confirmed the identity and purity of the obtained compound (34). **^{1}H-NMR** (300 MHz, DMSO-d6): δ (ppm) 3.12 (s,3H), 4.10 (s, 3H), 7.71 (t, 1H), 7.83 (t, 1H), 8.19 (d, 1H), 8.40 (d, 1H). **UPLC-ESI-MS** (positive mode) m/z: 196.0 (**4** + H$^+$)$^+$ a.m.u.

Synthesis of (Z)-1-(3-hydroxypropyl)-4-((3-methylbenzo[d]thiazol-2(3H) ylidene)methyl)quinolin-1-ium iodide (CyOH)

1-(3-Hydroxypropyl)-4-methylquinolinium iodide **2** (1 eq, 73.2 mg, 0.362 mmol) was reacted with 3-methyl-2-(methylthio)-1,3-benzothiazol-3-ium iodide **4** (1 eq, 65.9 mg, 0.362 mmol) in 1.5 mL ethanol containing 50.4 µL of triethylamine (TEA). After 90 min under stirring at r.t., the solvent was evaporated under vacuum and the solid repeatedly washed with diethyl ether. The crude was purified by preparative HPLC eluting with Method 2. The desired CyOH was obtained with 77% yield as a red solid. Comparison of the experimental with literature data confirmed the identity and purity of the obtained compound (31). **^{1}H-NMR** (300 MHz, DMSO-d6): δ (ppm) 2.01 (bs, 2H), 3.50 (bs, 2H), 4.02 (s, 3H), 4.66 (t, 2H), 4.82 (m, 1H, OH), 6.94 (s, 1H), 7.36-7.46 (m, 2H), 7.62 (t, 1H), 7.76-7.82 (m, 2H), 8.00-8.09 (m, 2H), 8.15 (d, 1H), 8.61 (d, 1H), 8.81 (d, 1H). **UPLC-ESI-MS** (positive mode) m/z: 349.5 (CyOH + H$^+$)$^+$ a.m.u.

Oligonucleotide, probe, and protein samples

The oligonucleotides: V7t1 (5'TGTGGGGGTGGACGGGCCGGGTAGA3'), 3R02 (5'TGTGGGGGTGGACTGGGTGGGTACC3') and V7t1-biotin (5'TGTGGGGGTGGACGGGCCGGGTAGA3'-biotin) were purchased from biomers.net GmbH (Germany). The oligomer identity and purity were confirmed by MALDI-TOF mass spectrometry and high-performance liquid chromatography (HPLC) data provided by the commercial supplier. The oligonucleotides were dissolved in Ultra-pure nuclease-free water (VWR) and their concentrations were determined by UV-vis analysis measuring the absorbance at 260 nm and 95 °C using the molar extinction coefficients ε = 280504 cm^{-1}M^{-1} and ε = 270124 cm^{-1}M^{-1} for V7t1 and 3R02, respectively. All the used aptamer solutions were obtained by proper dilution from a stock solution (1 mM) in the selected buffer, i.e. a pseudo-physiological Na$^+$-rich buffer (25 mM HEPES, 150 mM NaCl, pH 7.4), here indicated as HEPES/Na$^+$. Samples of annealed V7t1 and 3R02 were obtained by heating the appropriate oligonucleotide solutions at 95 °C for 5 min and leaving them to cool to r.t. overnight. Not-annealed (N.A.) and annealed (A.) V7t1 and 3R02 samples were then kept at 4 °C until use. The final compound CyOH was dissolved in Ultra-pure nuclease-free water (VWR) in all the experiments. Recombinant human $VEGF_{165}$ and His-tag labelled $VEGF_{165}$ ($VEGF_{165}$-His, GenScript) were purchased from Twin Helix Srl (Italy). Protein concentration was confirmed by Bradford assay (Bio-Rad) using Bovine Serum Albumin (BSA) as standard.

UV-vis spectroscopy experiments

The UV spectra were obtained on a Jasco V-750 UV-Vis spectrophotometer, using 1 cm path length cuvettes (1 mL internal volume, Hellma). The UV–vis spectra were recorded in the 230–650 nm range using a scanning speed of 100 nm/min with appropriate baseline subtraction. Titration experiments were carried out using independent solutions at a fixed concentration (8 µM) of CyOH in HEPES/Na^+ buffer. Increasing amounts of N.A. V7t1 or 3R02 up to 8 µM were used, taken from DNA stock solutions dissolved in HEPES/Na^+ buffer.

Gel electrophoresis experiments

Acrylamide/bis-acrylamide (19:1) 40% solution, glycerol, and GelGreen Nucleic Acid Stain were purchased from VWR. Ammonium persulfate (APS) and tetramethylethylenediamine (TEMED) were purchased from Sigma Aldrich. N.A. and A. V7t1 or 3R02 samples (3.6 µM) in HEPES/Na^+ buffer were loaded on 20% polyacrylamide gels with TBE 1x (Tris–borate–EDTA) as running buffer. The ligand CyOH was added at 1:1 DNA:probe ratio and incubated with the aptamers for 30 min at r.t. Just before loading, samples were supplemented with 5% glycerol, and gels were run at constant 80 V for 3 h at r.t., stained with GelGreen Nucleic Acid Stain (supplemented with 0.1 M NaCl, according to manufacturer's instructions) for 30 min, and visualized with a UV transilluminator (Bio-Rad ChemiDoc XRS). Each experiment was performed at least in triplicate.

Fluorescence spectroscopy experiments

Fluorescence spectra were recorded at 25 °C on HORIBA JobinYvon Inc. FluoroMax®-4 spectrofluorimeter equipped with F-3004 Peltier using a quartz cuvette with a 1 cm path length (Hellma). For the fluorescence titration experiments, the excitation wavelength was set at 504 nm. Spectra were recorded in the 515–750 nm range, with entrance and exit slit set at 3 nm. Titrations were carried out using independent solutions at a fixed concentration (2 µM) of the ligand in HEPES/Na^+ buffer. Increasing amounts of V7t1 or 3R02 up to 4.0 µM were used from DNA stock solutions dissolved in HEPES/Na^+ buffer. Thioflavin-T (ThT) displacement assay was performed by adding to preformed N.A. V7t1 or 3R02-ThT complexes in a 2:1 aptamer-probe ratio (4 µM of aptamer and 2 µM of ThT), increasing amounts of CyOH up to 2 eq with respect to the aptamer (8 µM concentration). The excitation wavelength was set at 450 nm and spectra were recorded in the 455–650 nm range, with entrance and exit slit set at 3 nm.

Determination of fluorescence quantum yield of V7t1-CyOH complexes in HEPES/Na^+

In order to determine the fluorescence quantum yield of CyOH alone and in the presence of the dimeric or monomeric V7t1 aptamer (N.A. or A. V7t1 in HEPES/Na^+), a solution of fluorescein dissolved in 0.1 M NaOH solution was used as the reference standard, having absorbance and emission in similar regions as the tested samples. A series of solutions at different concentrations were prepared for the standard, for CyOH alone, and for the V7t1-CyOH complexes (2:1 ratio) with maximum values of absorbance in the range from 0.01 to 0.1, in order to minimize re-absorption effects in the 1 cm fluorescence cuvette (35). All measurements were performed at 20 °C. Standard 1 cm quartz cells were used for the absorbance and fluorescence measurements. Both excitation and emission slit width was set at 2 nm. The excitation wavelength used for obtaining fluorescence spectra was 470 nm. Absorption spectra were recorded on a Jasco V-750 spectrophotometer. Fluorescence spectra were recorded on HORIBA JobinYvon Inc. FluoroMax®-4 spectrofluorimeter equipped with F-3004 Peltier.

The quantum yield of the V7t1-CyOH complexes in HEPES/Na^+ (Φ_x) was determined according to the following equation:

$$\Phi_x = \Phi_{st}\left(\frac{m_x}{m_{st}}\right)\left(\frac{\eta_x^2}{\eta_{st}^2}\right)$$

where Φ_{st} is the quantum yield of fluorescein in a 0.1 M NaOH solution (Φ_{st} = 95%), m_x is the slope of a linear fit for the integrated fluorescence intensity of CyOH alone or V7t1-CyOH complexes *vs*. absorbance, m_{st} is the slope of a linear fit for the integrated fluorescence intensity of fluorescein *vs*. absorbance, n_x is the refractive index of HEPES (ni = 1.33), n_{st} is the refractive index of a 0.1 M NaOH solution (n_{st} = 1.33) (36, 37).

Circular dichroism spectroscopy experiments

CD spectra and CD-monitored melting curves were recorded in a quartz cuvette with a path length of 1 cm (3 mL internal volume, Hellma) on a Jasco J-1500 spectropolarimeter equipped with a Jasco CTU-100 circulating thermostat unit. Spectra were registered at 25 °C in the 225–700 nm range with 2 s response, 200 nm/min scanning speed, and 2.0 nm bandwidth, corrected by subtraction of the background scan with buffer and averaged over 3 scans. The experiments were performed on N.A. and A. aptamer samples in HEPES/Na^+ buffer at a 2 µM concentration. CD

titration experiments were obtained by adding to fixed amounts of the DNA samples (2 μM conc.) increasing amounts of the probe up to 10 eq., corresponding to a 20 μM solution. For the melting experiments, the ellipticity at 263 nm was followed in the 15–90 °C range with a 1 °C/min scan rate. Each experiment was performed in duplicate.
For the singular value decomposition (SVD) analysis performed on N.A. and A. V7t1 or 3R02, the CD spectra were normalized to molar circular dichroism Δε = (M^{-1} cm^{-1}) using the equation $\Delta\varepsilon = \theta / (32980 \times C \times l)$. The resulting spectra were then analyzed using the advanced software developed by del Villar-Guerra et al (38).

Electrophoresis mobility shift assays (EMSA)
EMSA assays were performed according to reported procedures (8, 10), with minor modifications. In detail, 30 pmol of V7t1 or 3R02 were incubated with 30 pmol of CyOH and 40 pmol of $VEGF_{165}$ at 4° C for 30 min. Glycerol was added to the samples to a final concentration of 5% before loading. Electrophoresis was carried out at 45 V for 2.5 h on 7% polyacrylamide gels in 1× TAE (Tris-Acetate-EDTA), pH 7.8 (39). Gels were first visualized on a UV transilluminator (BioRad ChemiDoc XRS) with no staining and then stained for 30 min with GelGreen Nucleic Acid Stain (supplemented with 0.1 M NaCl). Each experiment was repeated at least twice.

Cell cultures and cytotoxicity
Human breast MCF-7 cancer cells were obtained from the American Type Culture Collection (ATCC, Manassas, VA, USA), and were cultured in Dulbecco's modified Eagle medium (DMEM). Non-tumorigenic human breast MCF-10A cells were also obtained from ATCC (CRL-10317™) and cultured in complete Mammary Epithelial Cell Growth Medium (MEGM, Bullet Kit, Lonza, Switzerland) supplemented with 100 ng/mL Cholera toxin (*Vibrio cholerae*) as previously described (40). Cytotoxic effects of CyOH and of the V7t1 or 3R02-CyOH complexes were evaluated by the (3-(4,5-dimethylthiazol-2-yl)-2,5 diphenyltetrazolium bromide) reduction inhibition assay (MTT) after 48 h. For this purpose, cells (3,000/well) were seeded into 96-well plates and treated with increasing concentrations of each compound (from 0 to 30 μM). Cell survival was determined by measuring the absorbance of blue formazan at 570 nm with an automatic plate reader and expressed as the percentage of viable cells with respect to control untreated cells. Three independent experiments were performed with triplicate determinations. For all the experimental points, *P < 0.05, **P < 0.01 or ***P < 0.001 were obtained for the control *vs.* the treated samples by performing Student's t-test analysis.

Analysis of cell internalization of CyOH and V7t1- or 3R02-CyOH by CLSM
Analyses were performed as previously described (41). MCF-7 and MCF-10A cells were seeded on glass coverslips in 24-well plates, grown to semi-confluency, and then incubated with 5 μM of each sample. After incubation, the cells were washed with PBS 1x and then fixed with 4% paraformaldehyde in PBS for 15 min at r.t. To stain nuclei and VEGF-A protein in MCF-7 and MCF-10A cells, we employed Hoechst (0.001 mg/mL) for 15 min at r.t. and α-VEGF-A antibody (1:1000) at 4 °C overnight, respectively. Upon incubations, cells were washed twice with PBS, mounted on coverslips, and then observed by using a confocal laser-scanning microscope Zeiss LSM 700 and a 63x oil objective. Hoechst (Hoechst 33342, Trihydrochloride, Trihydrate) and α-VEGF-A antibody (Anti-VEGF-A antibody, Alexa Fluor® 488, Abcam) were purchased from ThermoFisher Scientific.

Results and Discussion

V7t1-$VEGF_{165}$ chemiluminescence-based binding studies
In our previous studies we demonstrated, by EMSA experiments, that $VEGF_{165}$ bound with higher affinity V7t1 in a dimeric, parallel G4 conformation – predominant in N.A. aptamer samples prepared in HEPES/Na^+ buffer – than when in monomeric, mainly antiparallel-G4 form, adopted by the aptamer in A. samples (8). To confirm this finding using a different technique, also aiming at a quantitative determination of the affinity of $VEGF_{165}$ for N.A. vs. A. V7t1 in HEPES/Na^+ buffer, chemiluminescence-based protein binding assays were here performed. In these experiments, $VEGF_{165}$ carrying a His-tag label was immobilized into the wells of a copper-coated 96-well plate, and then 3'-biotinylated V7t1 samples in HEPES/Na^+, in both the N.A. and A. form, were incubated in parallel experiments with the anchored protein at different concentrations (steps 1 and 2, Fig. 1a). Successively, each well was treated with streptavidin-HRP, which bound to the aptamer thanks to the biotin-streptavidin high-affinity recognition (step 3, Fig. 1a). Finally, a specific ECL reagent, substrate of HRP, was added to each well producing a chemiluminescence signal proportional to the amount of V7t1 bound to $VEGF_{165}$ (steps 4 and 5, Fig. 1a). Interestingly, in the case of N.A. V7t1, we observed a strong binding between the aptamer and the target protein (Fig. 1b, black squares), with a K_d of ca. 33 nM calculated from fitting the chemiluminescence signal values as a function of the aptamer concentration (Fig. S1). In contrast, for A. V7t1 only a very weak chemiluminescence signal was observed, with data that did not allow extrapolating a K_d value (Fig. 1b, red dots). These results clearly demonstrated on a quantitative basis that the interaction between $VEGF_{165}$ and V7t1 is negligible when the aptamer is in monomeric form, and very strong when the aptamer is mainly in a dimeric G4 form, thus fully corroborating our previous qualitative findings (8). The obtained K_d

value for V7t1 is ca. one order of magnitude higher than the one previously reported in the literature for this aptamer. This discrepancy can be attributed to the different experimental techniques and conditions used to determine the affinity for the protein (7, 42), not impairing the overall reliability of these experiments and particularly the comparison between the relative binding capacity of the N.A. and A. aptamer. However, to verify that the presence of the biotin-linker appendage did not reduce the affinity of the aptamer for the protein, an EMSA experiment was carried out using 3'-biotinylated V7t1 with $VEGF_{165}$ under the same conditions previously reported for unmodified V7t1 (8). The experimental results were essentially like those obtained with unmodified V7t1, demonstrating that the introduction of the biotin-linker tether at the 3'-end of the V7t1 sequence did not alter the aptamer folding required for protein recognition (*vide infra*).

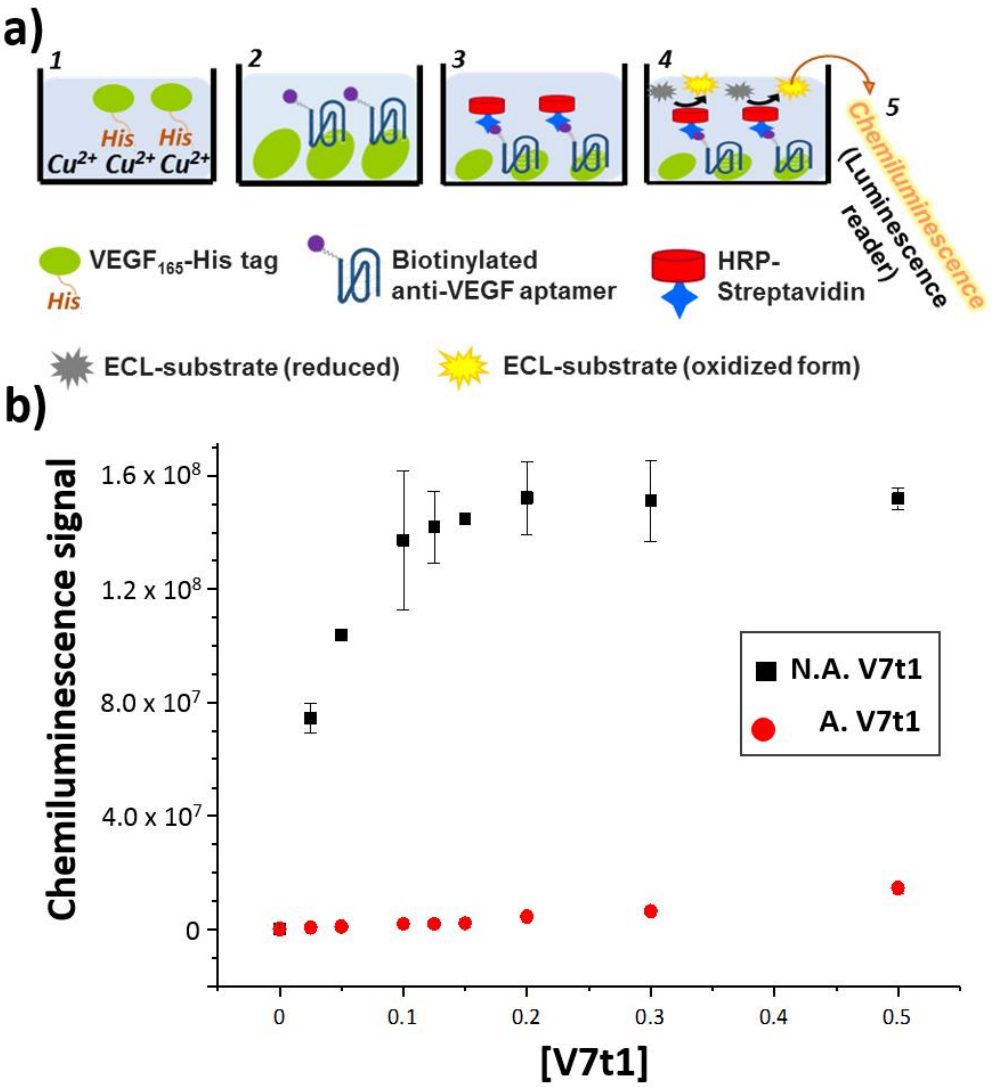

Figure 1. a) Schematic representation of the $VEGF_{165}$ binding assay on a copper-coated 96-well plate. b) Chemiluminescence signal reported as a function of the V7t1 aptamer concentration. Plotting is obtained by registering the chemiluminescence signals from fixed amounts of ECL/streptavidin-HRP added to increasing amounts of either N.A. or A. biotinylated V7t1 in HEPES/Na^+ pre-bound to 20 pmol of $VEGF_{165}$, previously immobilized on a 96-well plate. The black squares refer to N.A. V7t1 (predominantly dimeric G4 structure), the red dots refer to A. V7t1 (only monomeric G4 structure).

Synthesis of the cyanine dye CyOH

The cyanine CyOH, already known as a valuable fluorescent probe in the biological context (29–31, 43), was here selected to obtain a G4 ligand with even better recognition properties compared to TO but also reduced tendency to self-aggregate in solution. It maintains the central chromophore of TO, necessary for G-quartet recognition, and carries a propyl linker functionalized with a terminal hydroxyl group on the quinolinium ring of TO instead of the methyl group. The presence in the TO scaffold of a longer appendage, terminating with the polar hydroxyl group, should provide a ligand with better solubility in aq. solutions, lower aggregation propensity and with the ability to form additional hydrogen bonds with the target.

CyOH was prepared essentially following a literature protocol, which was modified by us to improve the reaction yields and simplify the working conditions. As first step, 4-methylquinoline **1** was alkylated with 3-iodopropan-1-ol in ethanol (Scheme 1, step a); this procedure was preferred to the use of the corresponding bromo derivative, thus leading to compound **2** in better yields (90%) compared to the previously reported ones (30). In parallel, benzothiazolium iodide **3** was reacted with methyl iodide to give 1-methylbenzothiazolium iodide **4** (Scheme 1, step b). The final condensation between **2** and **4** was carried out in ethanol, treating the reaction mixture with triethylamine (TEA) at r.t. for 90 min (Scheme 1, step c), adapting the procedure used for a similar substrate (44). The crude product CyOH was obtained as a precipitate by the addition of diethyl ether and was subsequently purified by HPLC. The final target compound was thus isolated in pure form with an overall yield of 77%, i.e. with a relevantly increased yield compared to the 20% previously reported in the literature (31).
Compounds **2**, **4**, and CyOH were analysed by analytical HPLC (Fig. S2), always showing > 95% purity, and characterized by UPLC-ESI-MS (Fig. S3) and ^{1}H-NMR analysis (Fig. S4), which fully confirmed their identity, also in comparison with literature data (31, 33, 34).

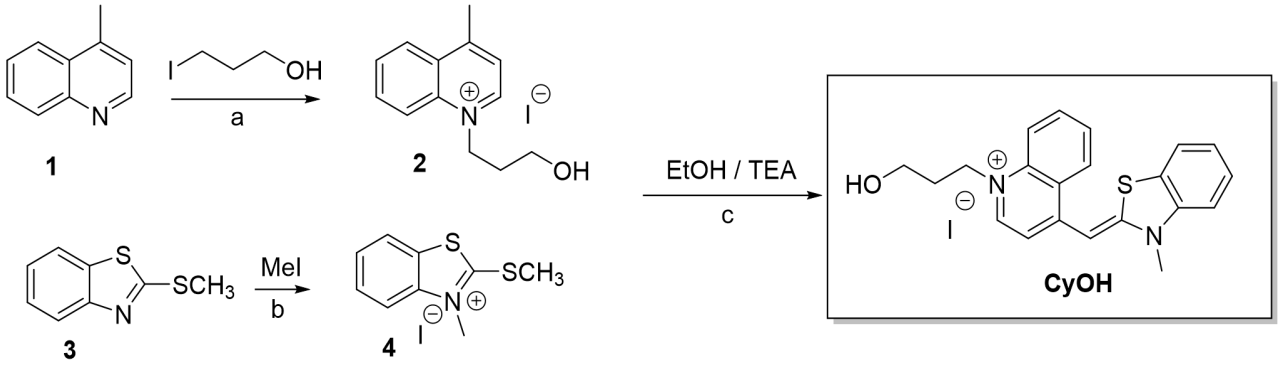

Scheme 1. Synthetic scheme for the preparation of the selected CyOH probe: a) 3-iodo-1-propanol in ethanol (2.5 eq.), reflux, 72 h; b) MeI (3 eq.), 100 °C, 15 h; c) EtOH/TEA, r.t., 90 min.

UV-vis spectroscopic analysis of CyOH and UV-monitored titrations of CyOH with V7t1 and 3R02

The absorption properties of the selected dye were analyzed by recording the UV-vis spectra of CyOH dissolved in water and in a pseudo-physiological Na^+-rich buffer (HEPES/Na^+) at various concentrations (from 4 to 36 µM, Fig. S5). CyOH showed a predominant band at 504 nm and a weaker vibronic shoulder at 476 nm, similarly to TO (45, 46). A linear trend, strictly following the Beer-Lambert law, was obtained by plotting the absorbance values of CyOH at 504 nm vs. concentration for both solvent systems, which allowed excluding the formation of aggregates of the dye in the studied conditions, even at the highest concentrations explored (Fig. S5). Moreover, the CyOH absorbance profiles proved to be similar in shape when recorded in methanol (data not shown) and in aq. buffers, further confirming the presence in aq. solution of the dye monomeric form (45, 46).
UV-monitored titrations were then carried out treating CyOH at a fixed concentration (8 µM) with increasing amounts of V7t1 or, in parallel experiments, of 3R02, previously annealed or not in HEPES/Na^+ buffer, as described in the experimental section, up to 8 µM. In the titration experiments, hypochromic effects were observed at very high CyOH/aptamer ratios, with intensity reduction of the band at 504 nm, then followed by progressive bathochromic shifts of the maxima to 516 nm for the N.A. and to 512 nm for the A. aptamers, and final hyperchromism, allowing to essentially recover most of the original CyOH signal intensity at CyOH/aptamer 1:1 ratio (Fig. S6). G4-induced hypochromicity in the UV spectrum of the dye is diagnostic of ligand binding to DNA through π-π stacking interactions (47, 48). These results, in accordance with the behaviour of other cyanine dyes known to interact in a monomeric form with G4 DNA, point to a binding with the aptamers in which CyOH - at CyOH/aptamer 1:1 ratio - targets the terminal G-quartets of G4 structures and is not self-aggregated (49–51).

Binding studies on the interaction of CyOH with V7t1 and 3R02 by polyacrylamide gel electrophoresis (PAGE) analysis

Native gel electrophoresis experiments were carried out to characterize the interaction of CyOH with N.A. and A. V7t1 in terms of number and molecularity of the species present in solution. All the experiments were performed by mixing the DNA and the probe at 1:1 ratio in the selected HEPES/Na^+ buffer. As previously observed (8), specific staining for nucleic acids (GelGreen) showed two main bands for N.A. V7t1, attributable to the presence of monomeric and dimeric G4 structures (Fig. 2, GelGreen, lane 1), whereas after annealing the retarded band disappeared, indicating that the dimeric species did not reform in the V7t1 sample after the heating/cooling cycle (Fig. 2, GelGreen, lane 3), in accordance with our previous findings (8). Interestingly, the addition of 1 eq. of CyOH to both N.A. and A. V7t1

samples produced no change in the molecularity of the systems as well as in the monomer/dimer ratio (Fig. 2, GelGreen, lanes 2 and 4).
Noteworthy, by simply visualizing the same gel with a UV transilluminator before adding the staining solution, a strong fluorescent signal was appreciated in correspondence to the retarded aptamer bands mixed with the probe (Fig. 2, No GelGreen, lane 2). Thus, CyOH gave a marked fluorescence light-up but only upon binding to dimeric V7t1. This result is particularly relevant considering that the dimeric form has a much higher affinity for $VEGF_{165}$ than the monomeric form, as demonstrated in our previous studies (8).
A titration experiment was also carried out adding increasing amounts of CyOH up to 2 eq. to N.A. V7t1 in HEPES/Na^+, showing increasing fluorescence intensity of the complex up to 1:1 CyOH-aptamer ratio, and then an essentially constant fluorescence intensity when in excess of the probe (Fig. S7).

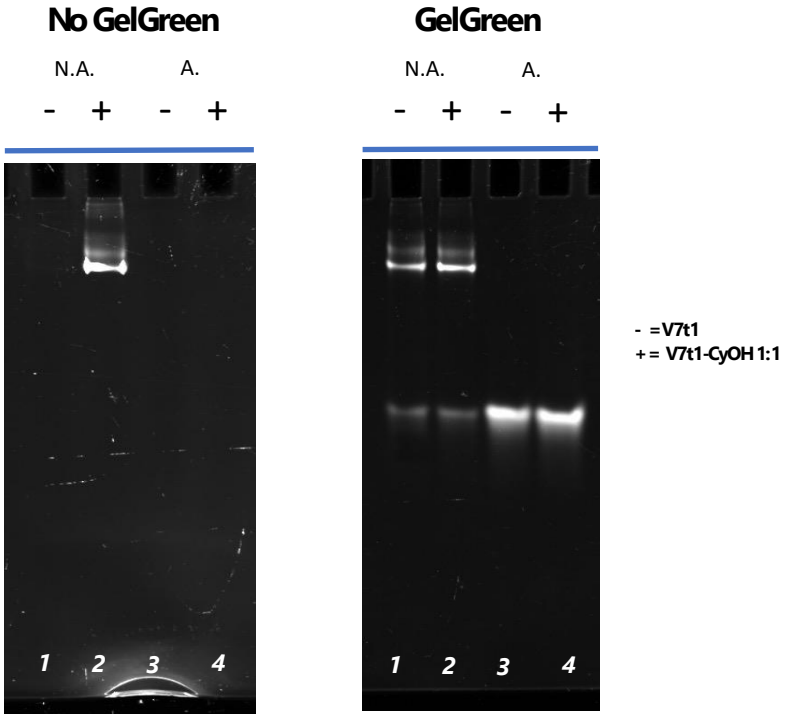

Figure 2. Representative 20% polyacrylamide gel electrophoresis analysis under native conditions of 3.6 µM V7t1 in HEPES/Na^+ buffer. The gel was run at constant 80 V for 3 h at r.t. with TBE 1x as running buffer. N.A. and A. V7t1 samples were loaded in lanes 1 and 3, respectively, whereas the 1:1 complexes of N.A. and A. V7t1 with CyOH were loaded in lanes 3 and 4, respectively.

The same experiments were also carried out to characterize 3R02, in both N.A. and A. form, in its interaction with CyOH at 1:1 DNA:probe ratio in HEPES/Na^+. Specific staining for nucleic acids (GelGreen) showed a band related to the presence of monomeric species for N.A. 3R02, along with multiple retarded bands, which is indicative of the presence of both dimeric and multimeric G4 structures (Fig. 3, GelGreen, lane 1). In analogy to what was observed for V7t1, in the A. 3R02 sample these retarded bands were not detected, indicating that after heating the dimeric and multimeric species did not reform upon cooling (Fig. 3, GelGreen, lane 2). Also in the case of 3R02, in both N.A. and A. form, the addition of 1 eq. of CyOH did not alter the molecularity and monomer/dimer ratio of the systems (Fig. 3, GelGreen, lanes 3 and 4). Interestingly, by visualizing the gel under UV transilluminator before staining it, a strong fluorescence signal was detected only in correspondence to the retarded bands, demonstrating a selective light-up of the probe when bound to the dimeric and higher-order species of 3R02 (Fig. 3, No GelGreen, lane 3).

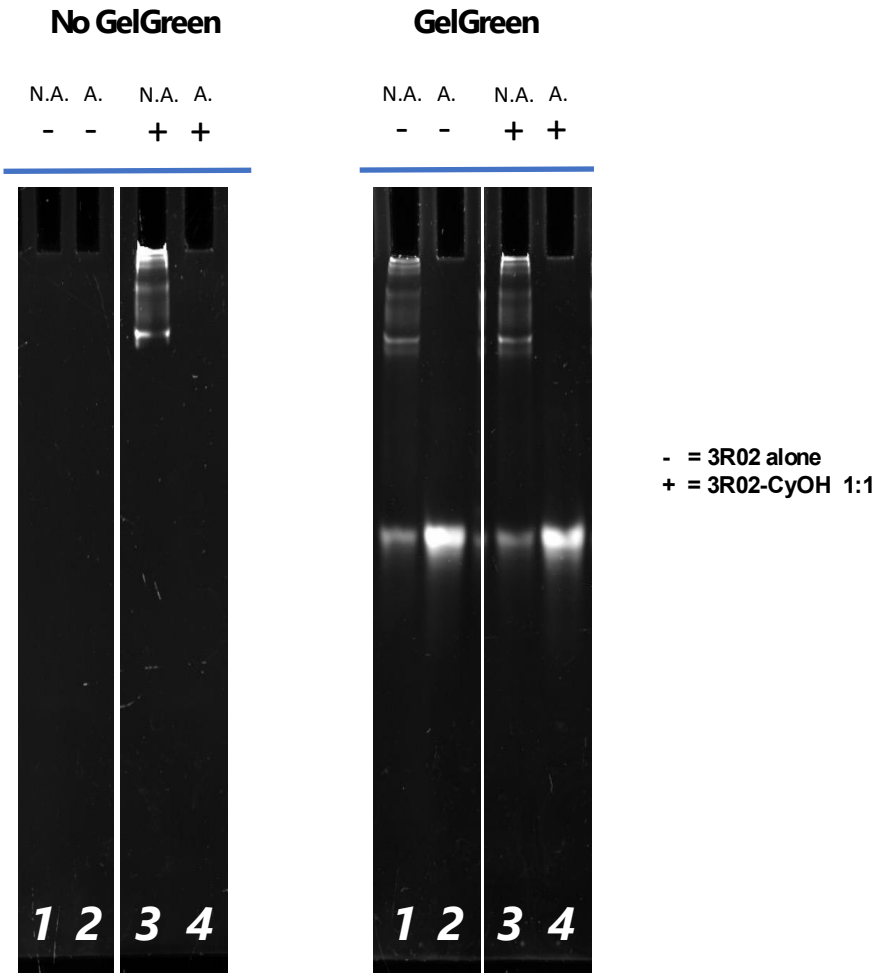

Figure 3. Representative 20% polyacrylamide gel electrophoresis analysis under native conditions of 3.6 μM 3R02 in HEPES/Na^+ buffer. The gel was run at constant 80 V for 3 h at r.t. with TBE 1x as running buffer. N.A. and A. 3R02 samples were loaded in lanes 1 and 2, respectively, whereas the 1:1 complexes with CyOH of the N.A. and A. 3R02 were loaded in lanes 3 and 4, respectively.

In order to confirm that the same behaviour was observed also in other pseudo-physiological solutions, and not only in the selected HEPES/Na^+, we also tested DMEM, a buffer typically used for cell assays. We thus performed a native gel loading N.A. V7t1 and 3R02 dissolved in DMEM, both with and without CyOH. The bands which appeared in this gel were exactly the same ones as found in HEPES/Na^+, demonstrating the predominant presence of the dimeric (and also multimeric for 3R02) aptamers and their selective fluorescence light-up in the presence of CyOH also under these solution conditions (Fig. S8).

Binding studies on the interaction of CyOH with V7t1 and 3R02 by fluorescence spectroscopy analysis

The interaction of CyOH with V7t1 and 3R02 was then studied by fluorescence spectroscopy analyzing both N.A. and A. aptamer samples. Fluorescence titrations were carried out at a fixed concentration of CyOH (2 μM) by adding increasing amounts of each aptamer, in the selected HEPES/Na^+ buffer, up to 4 μM. By exciting at 504 nm, CyOH alone showed a weak-to-null fluorescence signal (Fig. 4, black line), whereas, upon addition of the four aptamer systems in parallel experiments, a fluorescence band, with the maximum at 534 nm, appeared and progressively increased in intensity upon increasing the aptamer concentration (Fig. 4, colored lines). This result clearly confirmed that the probe interacted with both V7t1 and 3R02 aptamers, in their N.A. and A. forms, i.e. in both dimeric (also multimeric for 3R02) and monomeric forms. The fluorescence spectra had similar profiles in all cases (Fig. 4) suggesting a ligand-aptamer binding via π–π stacking interactions, in agreement with the UV-vis titration results (Fig. S6). Noteworthy, a very different fluorescence response of the probe was observed, with higher fluorescence light-up (around twice higher) when the probe interacted with the dimeric/multimeric G4s over the monomeric ones, in accordance with the PAGE analysis (Fig. 2 and 3).

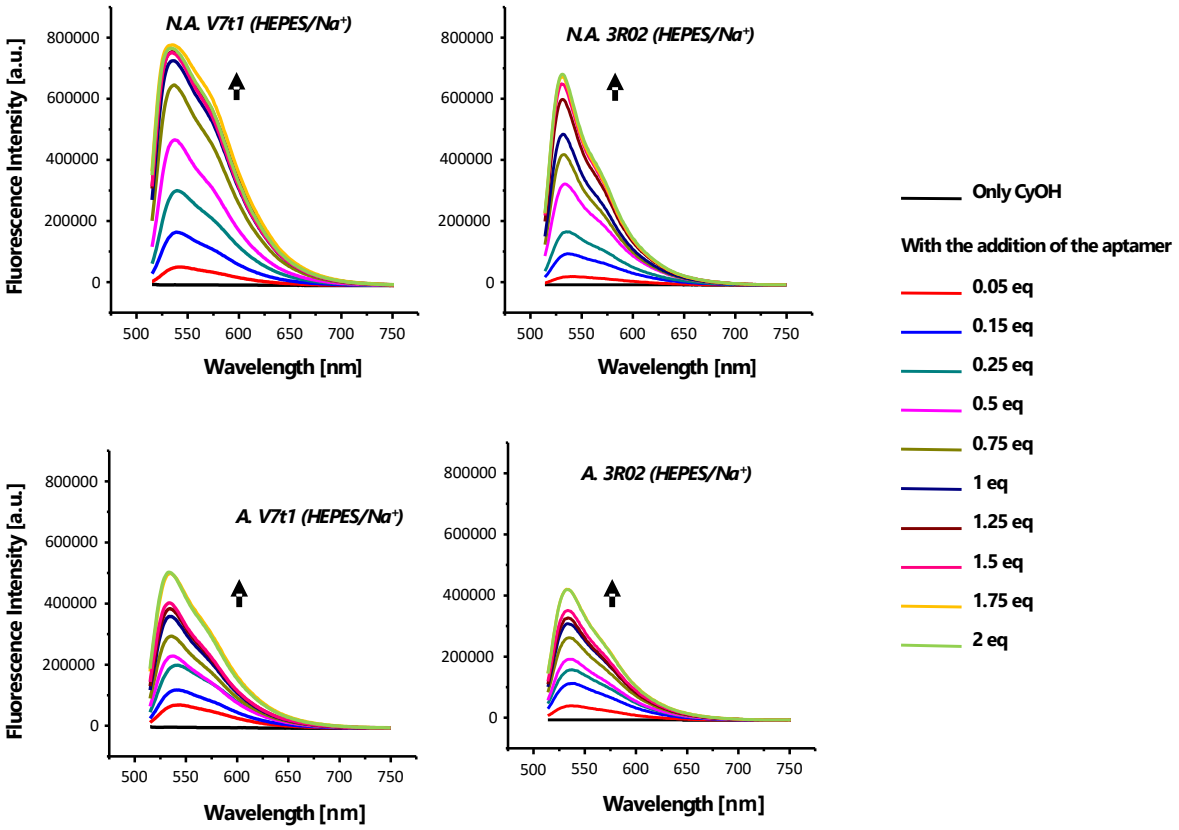

Figure 4. Representative fluorescence emission spectra obtained by adding increasing amounts of N.A. or A. V7t1 and 3R02 (from 0 to 2 eq.) to a 2 µM solution of CyOH (excitation wavelength: 504 nm, entrance and exit slit at 3 nm) in HEPES/Na^+ buffer.

To quantitatively describe the fluorescence enhancement associated with the binding of the selected cyanine to the studied aptamers, we determined the fluorescence quantum yield of CyOH alone and when bound in 1:1 ratio to N.A. or A. V7t1 in HEPES/Na^+, i.e. when the aptamer is mainly dimeric or only monomeric, respectively. By following the procedure described in the experimental section, we found that the ligand alone in solution has a very low fluorescence quantum yield (Φ_i = 0.02%), whereas relevant are the values obtained for the A. V7t1-CyOH (Φ_x = 14%) and N.A. V7t1-CyOH (Φ_x = 27%) complexes (Fig. S9). Thus, the fluorescence quantum yield value relative to the N.A. V7t1-CyOH 1:1 complex is ca. twice the one of the A. V7t1-CyOH complex, consistently with the fluorescence titration data, demonstrating on a quantitative basis the selective fluorescence light-up of the probe upon interaction with dimeric V7t1. Notably, the obtained fluorescence quantum yield for the N.A. V7t1-CyOH 1: 1 complex is perfectly in line with the values reported for the best fluorescent G4 ligands described in the literature, proving the remarkable efficiency of the here studied system (52, 53).

Competitive ThT binding assay

To further investigate the interaction mode of CyOH with the studied aptamers, we performed a fluorescence spectroscopy-based displacement assay using ThT as a model ligand. ThT is a known dye with almost null fluorescence when free in solution, able to give π-π stacking interactions on terminal G-quartets of G4 structures, which typically determine a fluorescence light-up signal (54–56). By adding increasing amounts of CyOH up to 2 eq (8 µM concentration) to the preformed N.A. or A. V7t1-ThT and 3R02-ThT 1:1 complexes, a dramatic decrease in the fluorescence signal of ThT was observed, with concomitant appearance of new fluorescence bands in the 525-550 nm region, compatible with the fluorescence emission of the aptamer-bound CyOH (Fig. S10). This finding clearly suggests that CyOH binds to the investigated aptamers essentially via the same binding mode used by ThT. Assuming π–π stacking interactions on terminal G-quartets of G4 structures as the main binding mode of CyOH on the target aptamers in both the N.A. and A. aptamers, CyOH proved to recognize the target G4 with higher affinity than ThT, displacing it from its preferred binding sites (57, 58).

Studies of the interaction between CyOH and V7t1/3R02 by CD spectroscopy analysis

To verify the effects of the probe binding on the aptamer G4 conformations CD analysis was performed. First, we recorded for both V7t1 and 3R02, either in the N.A. or A. form, CD spectra in the selected HEPES/Na^+ buffer (Fig. S11),

which, in the case of V7t1, agreed with those we previously reported in the same conditions (8). As far as 3R02 is concerned, we evidenced, analogously to V7t1, CD profiles indicative of mostly parallel G4 structures when in N.A. form, and mainly antiparallel G4 conformation after annealing, as confirmed by the deconvolution analysis reported in Fig S11. Then, we carried out titration experiments by adding increasing amounts of CyOH, up to 10 eq., to V7t1 or 3R02 taken at a fixed concentration (2 μM). The N.A. oligonucleotides showed, upon CyOH addition, very slight-to-null variation of the CD band centered at 263 nm, indicating that no detectable alteration of the parallel G4 folding of the aptamers occurred in the presence of the probe (8, 59). In contrast, upon addition of the probe to both V7t1 and 3R02 in their annealed form, a progressive decrease of the CD band centered at 299 nm, typical of antiparallel G4 structures, was observed, in concomitance with the increase of the maximum at 263 nm, thus indicating a net conformational switch – induced by the ligand in a concentration-dependent mode – of the target aptamers from mainly antiparallel to parallel G4 structures (Fig. 5 and S12) (59). This effect of CyOH on both monomeric A. aptamers, whose conformations are converted from antiparallel to parallel G4 structures, has been already reported in the literature for other ligands in the interaction with G4 structures. It is generally explained as the result of the more efficient ligand binding to the terminal G-quartets, due to more intense π-π stacking interactions, better exposed and thus more prone to binding in the case of parallel than antiparallel G4 structures (50, 60–62).

Interesting information on G-quadruplex/ligand interactions can be provided by verifying the presence of induced circular dichroism (ICD) signals, detected when a CD-inactive non-chiral ligand binds to a chiral host, as is a G4 structure, thus acquiring a CD signal due to its chiral environment (24). Analyzing the CD spectra of the titration experiments in the 225–600 nm range, marked ICD signals were evidenced only when CyOH was added in large excess to both N.A./A. V7t1 or 3R02 samples (Fig. 5). The CD profiles for all the investigated systems with CyOH-aptamer ratios higher than 2:1 showed a positive ICD band with a maximum centered at 516 nm and a negative ICD band with a minimum at 475 nm, more pronounced for the A. than for the N.A. aptamers (Fig. 5). The bisignate ICD signals indicate the aggregation of the dye when bound to the aptamers, with probably one type of aggregate, most likely dimeric, as suggested by the presence of a well-defined isodichroic point in the ICD bands (51, 63). The lower intensity of the ICD signals in the N.A. *vs.* A. V7t1/3R02 forms can be explained considering that when multiple ligand molecules bind the aptamers, the interaction with the dimeric aptamers occurs essentially via end-stacking onto the outer G-quartets of the dimer, whereas in the case of the monomeric ones, at high ligand ratios, in addition to end-stacking also binding at loops and/or grooves could be operative (51).

Effects on the thermal stability of the V7t1 and 3R02 G4 structures produced by CyOH binding were then analyzed by CD-melting experiments monitored at 263 nm at a 1:1 DNA:probe ratio (Fig. S13). N.A. V7t1 in HEPES/Na^+ showed a CD-melting profile with a clear stabilization effect in the presence of the ligand even though, similarly to the aptamer alone, a complete denaturation of its G4 structure was not obtained even at 90 °C and $T_{1/2}$ values could not be determined (8). Also N.A. 3R02 was stabilized by the presence of CyOH, with apparent $T_{1/2}$ > 80 °C. For both A. V7t1 and 3R02 aptamers in HEPES/Na^+, a CD-melting profile could not be obtained since at 1:1 DNA:probe ratio both the maxima, at 299 and 263 nm, were very low.

Taken together, the CD results demonstrated a strong interaction of CyOH with both V7t1 and 3R02, with a peculiar ability of the ligand to induce a conformational switch in the monomeric A. aptamers, converting the G4 structures from antiparallel into parallel, in excess of the probe, probably due to a more efficient stacking binding mode. The binding of CyOH to the target aptamers at high probe:DNA ratios showed marked and always progressively increasing ICD effects, which could be explained hypothesizing that additional ligand molecules can bind the preformed CyOH-aptamer 1:1 or 2:1 complex via simple CyOH-CyOH aggregation on the aptamer. Thus, different binding modes can be operative when the aptamers bind multiple CyOH molecules, and particularly loop/groove binding could be also considered for monomeric A. G4 structures, which show the highest ICD effects though showing the lowest fluorescence turn-on of the ligand.

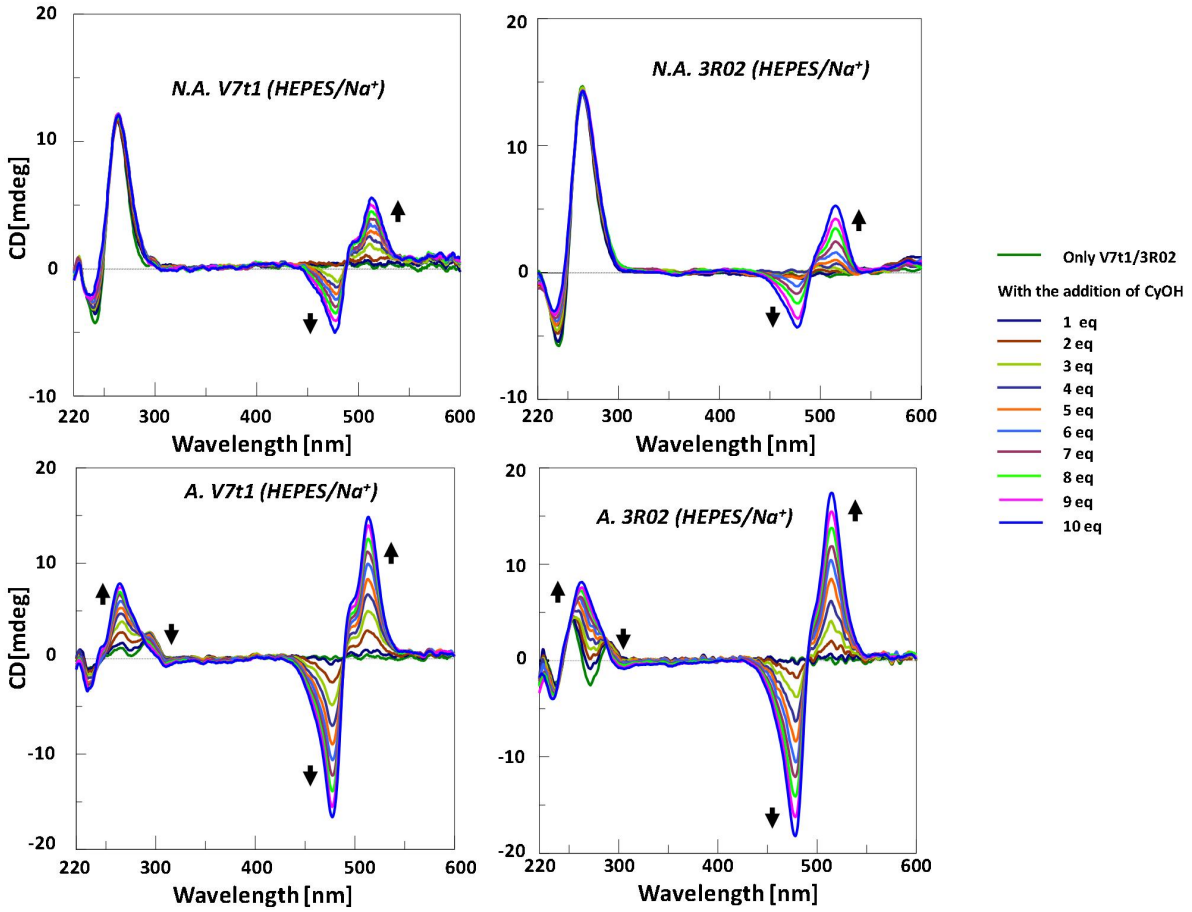

Figure 5. Overlapped representative CD spectra obtained by adding increasing amounts of CyOH (up to 10 eq.) to a 2 µM solution of V7t1/3R02 in HEPES/Na^+ buffer.

Electrophoretic analysis of V7t1/3R02-CyOH binding with the target $VEGF_{165}$

In order to verify if $VEGF_{165}$ was able to bind V7t1 also in the presence of CyOH and if the selective fluorescence light-up of the probe complexed with dimeric V7t1 was maintained upon protein binding, EMSA analyses under non-denaturing conditions were carried out (39). Both N.A. and A. V7t1 samples were incubated with 1 eq. CyOH and 1.3 eq. $VEGF_{165}$, analyzing the resulting mixtures by PAGE using the free oligonucleotide as control. GelGreen staining, able to reveal nucleic acids, showed that upon addition of the target protein only the bands corresponding to dimeric V7t1 completely disappeared, whereas no change was observed in both mobility and/or intensity of the faster migrating bands of monomeric V7t1. Thus, the addition of CyOH to V7t1 did not perturb the protein recognition ability of the aptamer (Fig. 6, GelGreen, lanes 3 and 4, and 9 and 10, respectively). Without gel staining, UV transilluminator evidenced the strong fluorescence signal of CyOH only in correspondence of a new retarded band, attributable to the aptamer-CyOH-protein complex in the sample containing N.A. V7t1, CyOH and $VEGF_{165}$ (Fig. 6, No GelGreen, lane 3). This result confirmed the strong preference of $VEGF_{165}$ for dimeric over monomeric V7t1 (8) also when the aptamer was bound to the selected cyanine probe.

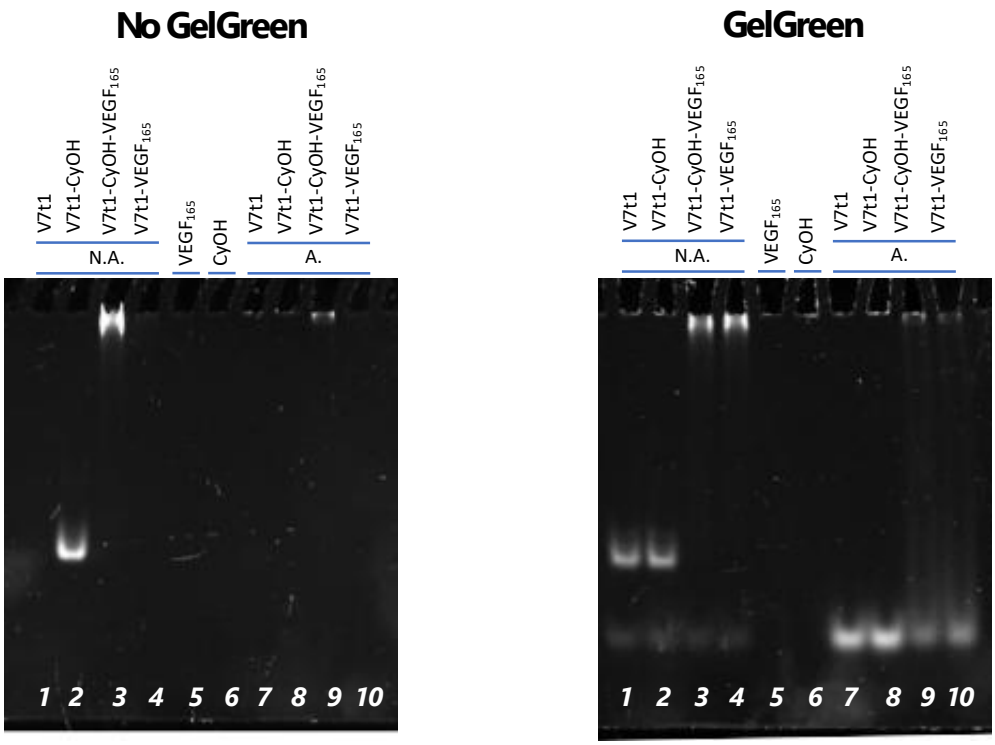

Figure 6. Representative unstained (No GelGreen) and GelGreen-stained EMSA of A. and N.A. V7t1 (30 pmol) incubated with CyOH (30 pmol) and $VEGF_{165}$ (40 pmol) in HEPES/Na^+ buffer. N.A. V7t1 was loaded in lanes **1-4** and A. V7t1 in lanes **7-10.** The gel was run at constant 45 V for 2.5 h with TAE 1x as running buffer.

An EMSA experiment carried out under the same conditions described above was performed also on the biotinylated V7t1 aptamer, here used for the experiments reported in Fig. 1 to determine the affinity for $VEGF_{165}$, demonstrating that the introduction of a biotin tag at the 3'-end of V7t1 did not impair the protein recognition abilities of the aptamer (Fig. S14).

In parallel, an EMSA experiment was performed also on 3R02 to verify the behaviour of this aptamer in the presence of the fluorescent probe and the target protein $VEGF_{165}$ (7). Both N.A. and A. samples of the aptamer were analysed in HEPES/Na^+, to compare the aptamer when essentially in dimeric/multimeric G4 form and when only monomeric. Both N.A. and A. 3R02 samples were incubated with 1 eq. CyOH and 1.3 eq. $VEGF_{165}$ and the resulting mixtures were analysed by PAGE using free 3R02 and V7t1 oligonucleotides as controls.

GelGreen staining showed the selective disappearance of all retarded bands of 3R02 (Fig. S15, GelGreen, *cfr*. lane 3 with 7, and lane 5 with 1), whereas only a very little change in the intensity of the faster-migrating bands of monomeric 3R02 was observed (*cfr*. lane 4 with 8, and lane 6 with 2). This slight difference in the behaviour of A. 3R02 compared to V7t1 – which under the tested conditions never showed the detectable formation of complexes with the protein by EMSA experiments – can be probably due to the higher affinity of 3R02 than V7t1 for the target protein (K_d = 0.3 *vs.* 1.4 nM) (7). Without GelGreen staining, it was possible to appreciate, under UV transilluminator, a strong fluorescence signal of the cyanine only in correspondence to the new retarded band attributable to the formation of the cyanine-aptamer-protein complex in the system containing N.A. 3R02, CyOH and $VEGF_{165}$ (Fig. S13, No GelGreen, lane 3). The multiple bands observed in N.A. 3R02 sample are probably dimers and multimers that, similarly to the dimeric V7t1, show a strong preference for $VEGF_{165}$ over monomeric 3R02. Even considering the higher polymorphism of 3R02 *vs*. V7t1, overall EMSA experiments showed similar behaviour for the two aptamers with the target protein. In fact, for both V7t1 and 3R02, the formation of aptamer/protein complexes in the presence of CyOH was easily revealed only with the dimeric or higher-order G4 structures of the selected aptamers.

Biological studies

To explore the effects on both cancer and normal cells of the V7t1/3R02-CyOH complexes, as well as their cellular internalization and ability to recognize $VEGF_{165}$ within the cells, cellular assays and confocal laser scanning microscopy (CLSM) experiments were performed.

Analysis of the cytotoxic effects of CyOH and V7t1/3R02-CyOH complexes on human cancer and normal cell lines

To evaluate the antiproliferative activity of V7t1/3R02-CyOH complexes on cancer and healthy cells in comparison with the free single compounds (*i.e.* V7t1, 3R02, CyOH), we performed *in vitro* experiments on the human breast

cancer MCF-7 cells, using the non-tumorigenic human MCF-10A cells as control, determining the cell viability by MTT assays (see experimental part). The obtained results indicated that CyOH alone exerted significant dose-dependent toxic effects on both cancer and normal cells, with similar IC_{50} values (28 and 30 µM, respectively) after 48 h incubation. Interestingly, when the aptamer-CyOH complexes were tested on the same cell lines, these systems proved to be much less toxic than the probe alone, particularly on the healthy cells. Cell viability of MCF-7 cells treated with V7t1-CyOH at 30 µM was ca. 60% and with 3R02-CyOH at the same concentration was ca. 75%, whereas under the same treatments MCF-10A cells always showed ca. 90% cell viability (Fig. 7). The aptamer-CyOH complexes overall showed selectivity for cancer over non-cancer cells and in most cases reproduced the bioactivity trend of the corresponding nude aptamer, indicating generally very high stability also in the cellular context, thus not releasing free CyOH within the cells.

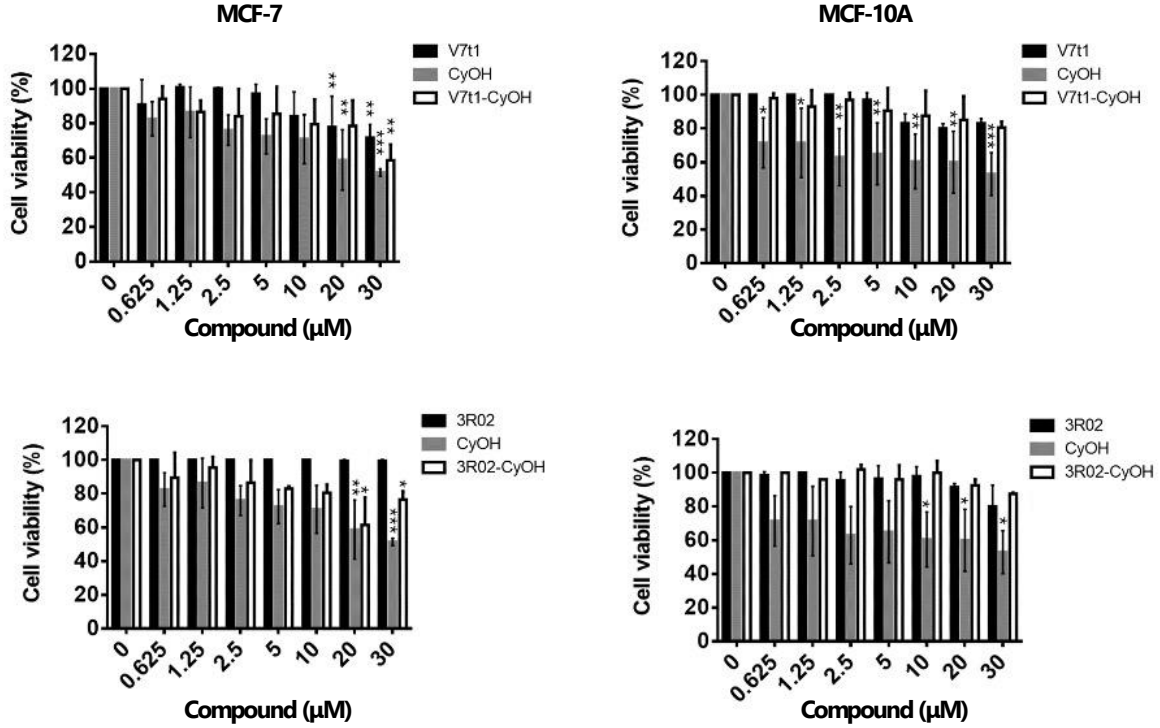

Figure 7. Effects of increasing concentrations of CyOH, nude aptamers and aptamer-CyOH complexes (0 - 30 µM) on the viability of human breast MCF-7 and non-tumorigenic breast MCF-10A cells upon 48 h of incubation. Cell viability values are expressed as the percentage of cell viability obtained for treated *vs.* control cells grown in the absence of the tested molecules. Three independent experiments were performed and, for all the experimental points, *P < 0.05, **P < 0.01 or ***P < 0.001 were obtained for treated *vs* control samples.

Analysis of CyOH and V7t1/3R02-CyOH complexes internalization into MCF-7 cells by CLSM

Time course experiments

To evaluate whether the effects detected on the tested cell lines were accompanied by effective cell internalization of CyOH and V7t1/3R02-CyOH complexes, CLSM experiments were performed. For this purpose, MCF-7 cancer cells were incubated at different times (3, 6, 9, 24, and 48 h) with each studied system at 5 µM, the concentration at which cell viability was always above 70%, and then analysed by CLSM using proper settings. As shown in Fig. 8, cell visualization performed by using settings suitable for Alexa Fluor 532 dye revealed that both CyOH and V7t1/3R02-CyOH complexes were taken up into cancer MCF-7 cells. However, CyOH alone entered cells very rapidly and in an unspecific manner, with clear toxic effects, in accordance with the MTT assay results. Indeed, upon this treatment, the cells appeared stressed and the nuclei were damaged after 24 and even more after 48 h (Fig. 8b). On the other hand, N.A. V7t1/3R02-CyOH were taken up by cells slower, with a significant internalization observed between 9 and 24 h incubation (Fig. 8c-d), exerting poor toxic activity in agreement with the MTT assay. This clearly demonstrated that the complexes were stable and did not dissociate within cells, allowing a selective transport of CyOH into cells bound to V7t1 and 3R02 aptamers.

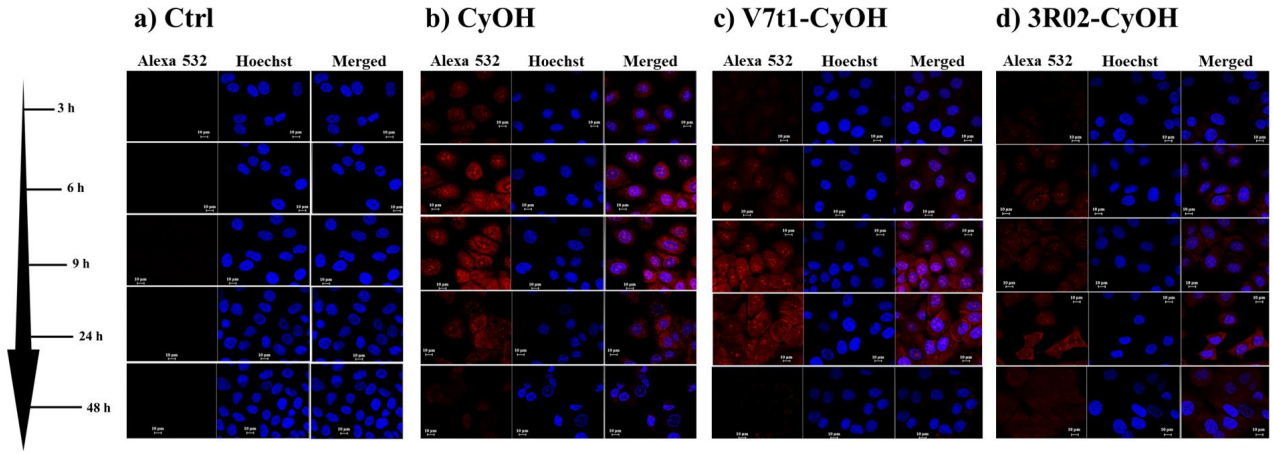

Figure 8. Confocal microscopy images relative to the internalization of CyOH and V7t1/3R02-CyOH complexes into MCF7 cells. a) control cells; b) cells incubated with CyOH; c) and d) cells incubated, respectively, with V7t1-CyOH and 3R02-CyOH complexes. In each panel, column 1 shows the visualization with the Alexa 532 filter suitable for the CyOH dye; column 2 the visualization with the Hoechst filter; column 3 the merge. Cells were cultured on glass coverslips in 24-well plates, grown to semiconfluency and incubated for 3, 6, 9, 24 and 48 h. Cell nuclei were stained by incubating the cells with 0.001 mg/mL Hoechst in PBS 1x for 20 min in the dark. After fixing the cells in 4% paraformaldehyde, these were analyzed by CLSM by using a 63X oil immersion objective.

Cellular colocalization experiments of CyOH and V7t1/3R02-CyOH complexes with $VEGF_{165}$

In order to evaluate whether the internalized aptamer complexes effectively target VEGF-A, cellular colocalization experiments were performed by CLSM on both human breast cancer MCF-7 and non-tumorigenic MCF-10A cells. For this purpose, immunofluorescence experiments were performed by incubating cells with 5 µM of V7t1/3R02-CyOH complexes for 24 h (i.e., the incubation time which allowed the best internalization of the complexes, as showed in the time course experiments in Fig. 8) and a fluorescently-labelled VEGF-A specific antibody to detect VEGF-A. Interestingly, CLSM analyses revealed different expression levels and localization of VEGF-A in normal and cancer cells. Indeed, in cancer MCF-7 cells, VEGF-A was found to be mainly present in the nuclei, whereas, in non-tumorigenic MCF-10A cells, it was mainly localized in the cytoplasm (Fig. 9, CTRL). Remarkably, the same localization pattern was found for both V7t1/3R02-CyOH complexes (Fig. 9, Alexa 532 columns), demonstrating a good colocalization with the fluorescent anti-VEGF-A antibody (Fig. 9, MCF-7 and MCF-10A panels, merged columns, 2^{nd} and 3^{rd} lines) and thus with the target VEGF-A. In the case of the MCF-7 cancer cells treated with V7t1/3R02-CyOH complexes, the fluorescence signal associated with the complexes was found to be mainly present in the nuclei (white arrows) and a strong colocalization with VEGF-A was detected (Fig. 9, yellow spots in MCF-7 panel, merged columns, 2^{nd} and 3^{rd} lines). For the healthy MCF-10A cells, the fluorescence of the complexes appeared mainly localized in the cytoplasm, with a good colocalization with the target VEGF-A (Fig. 9, yellow spots in MCF-10A panel, merged columns, 2^{nd} and 3^{rd} lines). In contrast, the probe alone did not follow the localization pattern of VEGF-A, nor one of the aptameric complexes (Fig. S16), corroborating the hypothesis that in these complexes, CyOH was tightly bound to V7t1 and 3R02 and was not released as such upon binding to the target protein, in accordance with EMSA experiments.

Overall, particularly in MCF-7 cells, in which a mainly nuclear localization of VEGF-A was evidenced, the efficacy of the V7t1/3R02-CyOH complexes as staining agents for VEGF-A detection appeared comparable to the one of the commercially available anti-VEGF-A antibody, thus confirming the potential of these aptamers in diagnostic applications.

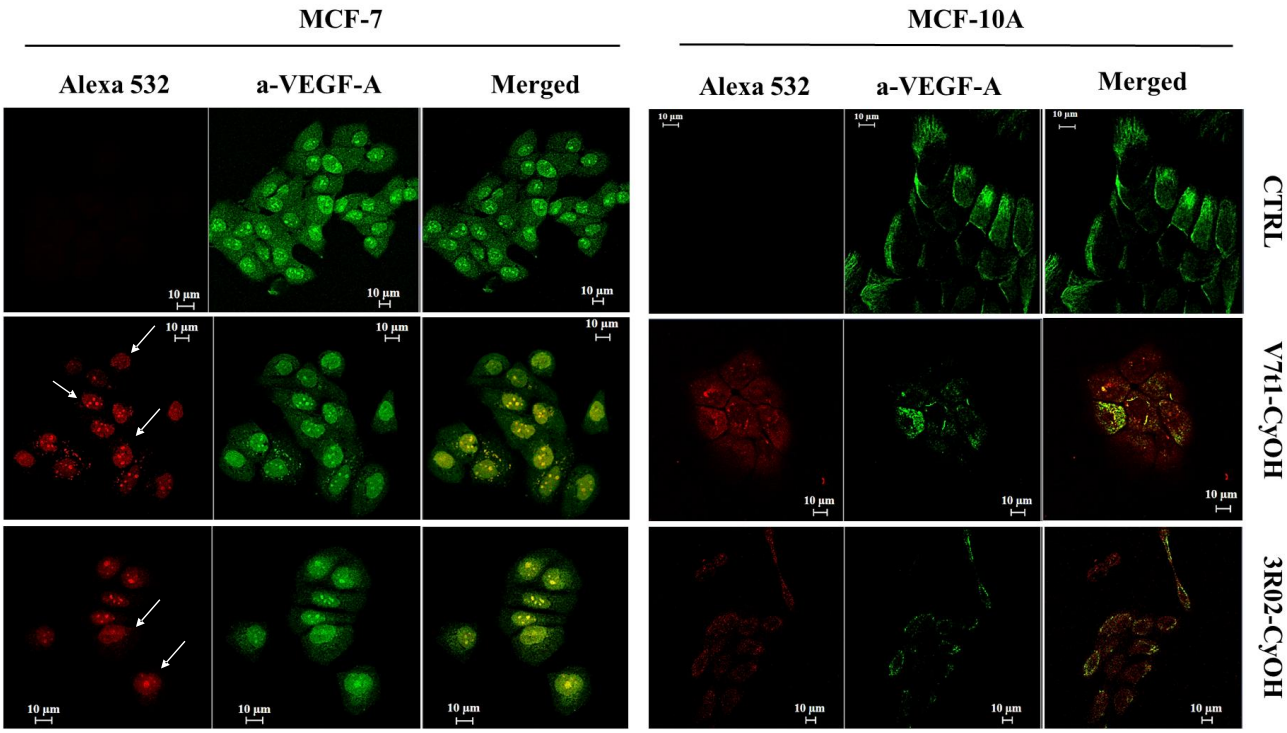

Figure 9. Confocal microscopy images relative to the internalization experiments on V7t1-CyOH and 3R02-CyOH into MCF-7 cells (left panel) and MCF-10A (right panel) cells. Cells were cultured on glass coverslips in 24-well plates, grown to semiconfluency and incubated for 24 h. VEGF-A was revealed by immunofluorescence experiments by using a fluorescent VEGF-A-specific antibody. After fixing the cells in 4% paraformaldehyde, these were analyzed by CLSM by using a 63X oil immersion objective.

Conclusions

We here described that the fluorescent cyanine probe CyOH is able to selective light-up when interacting with the dimeric/multimeric forms of the G4-forming anti-VEGF aptamers V7t1 and 3R02 (prevailing in not-annealed aptamer samples over their monomeric species, found in annealed samples), demostrating by gel electrophoresis and fluorescence titrations experiments. Interestingly, these dimeric/multimeric forms are recognized by the target protein with higher affinity than the monomeric species, as we demonstrated by EMSA and – representatively for V7t1 – also by chemiluminescence-based protein binding experiments. An in-depth biophysical characterization of the aptamer-CyOH complexes was carried out using a combination of spectroscopic (UV-vis, CD, and fluorescence spectroscopy) and electrophoretic (native PAGE) techniques, which – notwithstanding the intrinsic complexity of the aptamer systems – allowed defining their main features and particularly those of the 1:1 complexes, very stable and with a high fluorescence response when bound to the target protein. Indeed, the strong fluorescence light-up of CyOH upon interaction with dimeric aptamers *vs*. the modest fluorescence response observed with the monomeric aptamers could be explained by the formation of different structural complexes. In all cases π-π stacking interactions with the terminal G-quartets were responsible for the ligand binding but in the case of binding to monomeric aptamers, which in 1:1 complexes are essentially antiparallel G4 structures, higher exposure of CyOH to the polar solvent can be envisaged. In turn, more efficient stacking interactions and lower exposure to the polar solvent can be considered in the binding of CyOH to dimeric parallel G4 aptamers. In addition, it should be considered that in the case of the dimeric species, mixing the ligand and the oligonucleotide in 1:1 ratio would essentially provide complexes in which 2 ligand molecules are terminally bound per each dimeric aptamer unit.

Cellular experiments showed that, while CyOH alone exerted significant and similar dose-dependent toxic effects on both human MCF-7 cancer cells and non-cancerogenic MCF10-A cells, the aptamer-CyOH complexes proved to be much less toxic than the probe alone, particularly on the healthy cells, as determined by MTT assays. Indeed, aptamer-CyOH complexes showed selectivity for cancer over non-cancer cells and in most cases reproduced the bioactivity trend of the corresponding nude aptamer, indicating generally very high stability of these complexes also in the cellular context, not releasing free CyOH within the cells.

Time course experiments combined with CLSM revealed that these complexes were efficiently taken up into cancer MCF-7 cells, with a significant internalization observed between 9 and 24 h incubation, exerting poor toxic activity at the tested concentration (5 μM) in agreement with MTT assays.

Colocalization experiments with a fluorescently-labelled anti-VEGF-A antibody finally confirmed the effective ability of both V7t1-CyOH and 3R02-CyOH complexes to recognize the target protein, allowing its detection with high efficiency by exploiting the strong fluorescence of the probe.

These findings provide fundamental information to develop valuable and highly selective targeting agents for both diagnostic and theranostic applications. V7t1-CyOH and 3R02-CyOH complexes, in fact, represent an interesting proof-of-concept, being a valuable alternative to fluorescent antibodies, as well as to aptamers covalently conjugated to specific fluorescent probes, in which the insertion of the linker connecting the probe may affect the aptamer folding and thus the protein recognition ability. Studies to further optimize non-covalent dimeric aptamer-based complexes are currently underway in our laboratories to produce potential G-quadruplex-based drugs (64) and/or biosensors (65) for, respectively, *in vivo* and *ex vivo* applications.

Acknowledgements

D.M. thanks AIRC for financial support (grant IG2020 n. 25046 to D.M.). C.R. was supported by a fellowship from AIRC.

References

1. Melincovici,C.S., Boşca,A.B., Şuşman,S., Mărginean,M., Mihu,C., Istrate,M., Moldovan,I.M., Roman,A.L. and Mihu,C.M. (2018) Vascular endothelial growth factor (VEGF) – key factor in normal and pathological angiogenesis. *Rom. J. Morphol. Embryol.*, **59**, 455–467.
2. Takahashi,H. and Shibuya,M. (2005) The vascular endothelial growth factor (VEGF)/VEGF receptor system and its role under physiological and pathological conditions. *Clin. Sci.*, **109**, 227–241.
3. Ng,Y.S., Krilleke,D. and Shima,D.T. (2006) VEGF function in vascular pathogenesis. *Exp. Cell Res.*, **312**, 527–537.
4. Medford,A.R.L., Douglas,S.K., Godinho,S.I.H., Uppington,K.M., Armstrong,L., Gillespie,K.M., van Zyl,B., Tetley,T.D., Ibrahim,N.B.N. and Millar,A.B. (2009) Vascular Endothelial Growth Factor (VEGF) isoform expression and activity in human and murine lung injury. *Respir. Res.*, **10**, 1–12.
5. Riccardi,C., Napolitano,E., Platella,C., Musumeci,D. and Montesarchio,D. (2020) Anti-VEGF DNA-based aptamers in cancer therapeutics and diagnostics. *Med. Res. Rev.*, 10.1002/med.21737.
6. Nonaka,Y., Sode,K. and Ikebukuro,K. (2010) Screening and improvement of an anti-VEGF DNA aptamer. *Molecules*, **15**, 215–225.
7. Nonaka,Y., Yoshida,W., Abe,K., Ferri,S., Schulze,H., Bachmann,T.T. and Ikebukuro,K. (2013) Affinity improvement of a VEGF aptamer by in silico maturation for a sensitive VEGF-detection system. *Anal. Chem.*, **85**, 1132–1137.
8. Moccia,F., Riccardi,C., Musumeci,D., Leone,S., Oliva,R., Petraccone,L. and Montesarchio,D. (2019) Insights into the G-rich VEGF-binding aptamer V7t1: when two G-quadruplexes are better than one! *Nucleic Acids Res.*, **47**, 8318–8331.
9. Riccardi,C., Napolitano,E., Musumeci,D. and Montesarchio,D. (2020) Dimeric and multimeric DNA aptamers for highly effective protein recognition. *Molecules*, **25**, 7–15.
10. Riccardi,C., Musumeci,D., Platella,C., Gaglione,R., Arciello,A. and Montesarchio,D. (2020) Tuning the polymorphism of the anti-VEGF G-rich V7t1 aptamer by covalent dimeric constructs. *Int. J. Mol. Sci.*, **21**, 1–24.
11. Marušič,M., Veedu,R.N., Wengel,J. and Plavec,J. (2013) G-rich VEGF aptamer with locked and unlocked nucleic acid modifications exhibits a unique G-quadruplex fold. *Nucleic Acids Res.*, **41**, 9524–9536.
12. Sun,Z.Y., Wang,X.N., Cheng,S.Q., Su,X.X. and Ou,T.M. (2019) Developing novel G-quadruplex ligands: from interaction with nucleic acids to interfering with nucleic acid–protein interaction. *Molecules*, **24**, 396.
13. Umar,M.I., Ji,D., Chan,C.Y. and Kwok,C.K. (2019) G-quadruplex-based fluorescent turn-on ligands and aptamers: from development to applications. *Molecules*, **24**, 2416.
14. Kumar,R., Chand,K., Bhowmik,S., Das,R.N., Bhattacharjee,S., Hedenström,M., Hedenström,H. and Chorell,E. (2020) Subtle structural alterations in G-quadruplex DNA regulate site specificity of fluorescence light-up probes. *Nucleic Acids Res.*, **48**, 1108–1119.
15. Karg,B., Funke,A., Ficht,A., Sievers-Engler,A., Lämmerhofer,M. and Weisz,K. (2015) Molecular recognition and visual detection of G-quadruplexes by a dicarbocyanine dye. *Chemistry.*, **21**, 13802–13811.
16. Chen,X., Wang,J., Jiang,G., Zu,G., Liu,M., Zhou,L. and Pei,R. (2016) The development of a light-up red-emitting fluorescent probe based on a G-quadruplex specific cyanine dye. *RSC Adv.*, **6**, 70117–70123.
17. Ihmels,H., Jiang,S., Mahmoud,M.M.A., Schönherr,H., Wesner,D. and Zamrik,I. (2018) Fluorimetric detection of G-quadruplex DNA in solution and adsorbed on surfaces with a selective trinuclear cyanine dye. *Langmuir*, **34**, 11866–11877.
18. Wang,Y.Q., Hu,M.H., Guo,R.J., Chen,S. Bin, Huang,Z.S. and Tan,J.H. (2018) Tuning the selectivity of a commercial cyanine nucleic acid dye for preferential sensing of hybrid telomeric G-quadruplex DNA. *Sens. Actuators B Chem.*, **266**, 187–194.
19. Zhao,Z., Cao,S., Li,H., Li,D., He,Y., Wang,X., Chen,J., Zhang,S., Xu,J. and Knutson,J.R. (2022) Ultrafast excited-state

dynamics of thiazole orange. *Chem. Phys.*, **553**, 1–16.
20. Largy,E., Hamon,F. and Teulade-Fichou,M.P. (2011) Development of a high-throughput G4-FID assay for screening and evaluation of small molecules binding quadruplex nucleic acid structures. *Anal. Bioanal. Chem.*, **400**, 3419–3427.
21. Biancardi,A., Biver,T., Marini,A., Mennucci,B. and Secco,F. (2011) Thiazole orange (TO) as a light-switch probe: combined quantum-mechanical and spectroscopic study. *Phys. Chem. Chem. Phys.*, **13**, 12595–12602.
22. Owens,E.A., Huynh,H.T., Stroeva,E.M., Barman,A., Ziabrev,K., Paul,A., Nguyen,S. V., Laramie,M., Hamelberg,D., Germann,M.W., *et al.* (2019) Second generation G-quadruplex stabilizing trimethine cyanines. *Bioconjugate Chem.*, **30**, 2647–2663.
23. Yang,Q., Xiang,J., Yang,S., Li,Q., Zhou,Q., Guan,A., Zhang,X., Zhang,H., Tang,Y. and Xu,G. (2009) Verification of specific G-quadruplex structure by using a novel cyanine dye supramolecular assembly: II. The binding characterization with specific intramolecular G-quadruplex the recognizing mechanism. *Nucleic Acids Res.*, **38**, 1022–1033.
24. Sun,H., Tang,Y., Xiang,J., Xu,G., Zhang,Y., Zhang,H. and Xu,L. (2006) Spectroscopic studies of the interaction between quercetin and G-quadruplex DNA. *Bioorg. Med. Chem. Lett.*, **16**, 3586–3589.
25. Li,Z., Tan,J.H., He,J.H., Long,Y., Ou,T.M., Li,D., Gu,L.Q. and Huang,Z.S. (2012) Disubstituted quinazoline derivatives as a new type of highly selective ligands for telomeric G-quadruplex DNA. *Eur. J. Med. Chem.*, **47**, 299–311.
26. Kim,M.Y., Vankayalapati,H., Shin-Ya,K., Wierzba,K. and Hurley,L.H. (2002) Telomestatin, a potent telomerase inhibitor that interacts quite specifically with the human telomeric intramolecular G-quadruplex. *J. Am. Chem. Soc.*, **124**, 2098–2099.
27. Han,F.X., Wheelhouse,R.T. and Hurley,L.H. (1999) Interactions of TMPyP4 and TMPyP2 with quadruplex DNA. Structural basis for the differential effects on telomerase inhibition. *J. Am. Chem. Soc.*, **121**, 3561–3570.
28. Mita,H., Ohyama,T., Tanaka,Y. and Yamamoto,Y. (2006) Formation of a complex of 5,10,15,20-Tetrakis(N-methylpyridinium-4-yl)-21H,23H-porphyrin with G-Quadruplex DNA. *Biochemistry.*, **45**, 6765–6772.
29. Bieniarz,C., Huff,J.B. and Henrard,D. (1995) PCT Int. Appl.
30. Dempcy,R.O., Afonina,I.A. and Vermeulen,N.M.J. (2001) PCT Int. Appl.
31. Menacher,F., Rubner,M., Berndl,S., Wagenknecht,H. and Uni,V. (2008) Thiazole orange and Cy3: improvement of fluorescent DNA probes with use of short range electron transfer. *J. Org. Chem.*, **73**, 4263-4266.
32. Giancola,C. and Pagano,B. (2013) Energetics of ligand binding to G-quadruplexes. *Top. Curr. Chem.*, **330**, 211–242.
33. Wang,M.Q., Xu,J., Zhang,L., Liao,Y., Wei,H., Yin,Y.Y., Liu,Q. and Zhang,Y. (2019) Tuning the selectivity of N-alkylated styrylquinolinium dyes for sensing of G-quadruplex DNA. *Bioorg. Med. Chem.*, **27**, 552–559.
34. Lai,H.P., Gao,R.C., Huang,C.L., Chen,I.C. and Tan,K.T. (2015) Fluorescence switchable probes based on a molecular rotor for selective detection of proteins and small molecules. *Chem. Commun.*, **51**, 16197–16200.
35. Dhami,S., Mello,A.J.D., Rumbles,G., Bishop,S.M., Phillips,D. and Beeby,A. (1995) Phthalocyanine fluorescence at high concentration: dimers or reabsorption effect? *Photochem. Photobiol.*, **61**, 341–346.
36. Rhys Williams,A.T., Winfield,S.A. and Miller,J.N. (1983) Relative fluorescence quantum yields using a computer-controlled luminescence spectrometer. *Analyst*, **108**, 1067–1071.
37. Würth,C., Grabolle,M., Pauli,J., Spieles,M. and Resch-Genger,U. (2013) Relative and absolute determination of fluorescence quantum yields of transparent samples. *Nat. Protoc.*, **8**, 1535–1550.
38. del Villar-Guerra,R., Trent,J.O. and Chaires,J.B. (2018) G-Quadruplex secondary structure sbtained from circular dichroism spectroscopy. *Angew. Chem. Int. Ed. Engl.*, **57**, 7171–7175.
39. Hellman,L.M. and Fried,M.G. (2007) Electrophoretic mobility shift assay (EMSA) for detecting protein-nucleic acid interactions. *Nat. Protoc.*, **2**, 1849–1861.
40. Gaglione,R., Smaldone,G., Di Girolamo,R., Piccoli,R., Pedone,E. and Arciello,A. (2018) Cell milieu significantly affects the fate of AApoAI amyloidogenic variants: predestination or serendipity? *Biochim. Biophys. Acta - Gen. Subj.*, **1862**, 377–384.
41. Lampitella,E., Landi,N., Oliva,R., Gaglione,R., Bosso,A., de Lise,F., Ragucci,S., Arciello,A., Petraccone,L., Pizzo,E., *et al.* (2021) Toxicity and membrane perturbation properties of the ribotoxin-like protein Ageritin. *J. Biochem.*, **170**, 473–482.
42. Lönne,M., Bolten,S., Lavrentieva,A., Stahl,F., Scheper,T. and Walter,J.G. (2015) Development of an aptamer-based affinity purification method for vascular endothelial growth factor. *Biotechnol. Rep.*, **8**, 16–23.
43. Deligeorgiev,T.G., Gadjev,N.I., Drexhage,K.H. and Sabnis,R.W. (1995) Preparation of intercalating dye thiazole orange and derivatives. *Dye. Pigm.*, **29**, 315–322.
44. Stadler,A.L., Delos Santos,J.O., Stensrud,E.S., Dembska,A., Silva,G.L., Liu,S., Shank,N.I., Kunttas-Tatli,E., Sobers,C.J., Gramlich,P.M.E., *et al.* (2011) Fluorescent DNA nanotags featuring covalently attached intercalating dyes: Synthesis, antibody conjugation, and intracellular imaging. *Bioconjugate Chem.*, **22**, 1491–1502.
45. Nygren,J., Svanvik,N. and Kubista,M. (1998) The interactions between the fluorescent dye thiazole orange and DNA. *Biopolymers*, **46**, 39–51.

46. Guo,R.J., Yan,J.W., Chen,S. Bin, Gu,L.Q., Huang,Z.S. and Tan,J.H. (2016) A simple structural modification to thiazole orange to improve the selective detection of G-quadruplexes. *Dye. Pigm.*, **126**, 76–85.
47. Guan,A.J., Zhang,X.F., Sun,X., Li,Q., Xiang,J.F., Wang,L.X., Lan,L., Yang,F.M., Xu,S.J., Guo,X.M., *et al.* (2018) Ethyl-substitutive Thioflavin T as a highly-specific fluorescence probe for detecting G-quadruplex structure. *Sci. Rep.*, **8**, 1–12.
48. Verma,S., Ghuge,S.A., Ravichandiran,V. and Ranjan,N. (2019) Spectroscopic studies of Thioflavin-T binding to c-Myc G-quadruplex DNA. *Spectrochim. Acta - Part A Mol. Biomol. Spectrosc.*, **212**, 388–395.
49. Mahmood,T., Paul,A. and Ladame,S. (2010) Synthesis and spectroscopic and DNA-binding properties of fluorogenic acridine-containing cyanine dyes. *J. Org. Chem.*, **75**, 204–207.
50. Ihmels,H., Mahmoud,M.M.A. and Patrick,B.O. (2017) Optical differentiation between quadruplex DNA and duplex DNA with a [2.2.2]heptamethinecyanine dye. *J. Phys. Org. Chem.*, **30**, 1–9.
51. Mikulin,I., Ljubić,I., Piantanida,I., Vasilev,A., Mondeshki,M., Kandinska,M., Uzelac,L., Martin-Kleiner,I., Kralj,M. and Tumir,L.M. (2021) Polycationic monomeric and homodimeric asymmetric monomethine cyanine dyes with hydroxypropyl functionality—strong affinity nucleic acids binders. *Biomolecules*, **11**, 1–20.
52. Doria,F., Manet,I., Grande,V., Monti,S. and Freccero,M. (2013) Water-soluble naphthalene diimides as singlet oxygen sensitizers. *J. Org. Chem.*, **78**, 8065–8073.
53. Vummidi,B.R., Alzeer,J. and Luedtke,N.W. (2013) Fluorescent probes for G-quadruplex structures. *ChemBioChem*, **14**, 540–558.
54. Mohanty,J., Barooah,N., Dhamodharan,V., Harikrishna,S., Pradeepkumar,P.I. and Bhasikuttan,A.C. (2013) Thioflavin T as an efficient inducer and selective fluorescent sensor for the human telomeric G-quadruplex DNA. *J. Am. Chem. Soc.*, **135**, 367–376.
55. Gabelica,V., Maeda,R., Fujimoto,T., Yaku,H., Murashima,T., Sugimoto,N. and Miyoshi,D. (2013) Multiple and cooperative binding of fluorescence light-up probe thioflavin T with human telomere DNA G-quadruplex. *Biochemistry*, **52**, 5620–5628.
56. De La Faverie,A.R., Guédin,A., Bedrat,A., Yatsunyk,L.A. and Mergny,J.L. (2014) Thioflavin T as a fluorescence light-up probe for G4 formation. *Nucleic Acids Res.*, **42**, 1–8.
57. Livendahl,M., Jamroskovic,J., Ivanova,S., Demirel,P., Sabouri,N. and Chorell,E. (2016) Design and synthesis of 2,2′-diindolylmethanes to selectively target certain G-quadruplex DNA structures. *Chem.Eur.J.*, **22**, 13004–13009.
58. Jamroskovic,J., Livendahl,M., Eriksson,J., Chorell,E. and Sabouri,N. (2016) Identification of compounds that selectively stabilize specific G-quadruplex structures by using a thioflavin T-displacement assay as a tool. *Chem.Eur.J.*, **22**, 18932–18943.
59. Karsisiotis,A.I., Hessari,N.M.A., Novellino,E., Spada,G.P., Randazzo,A. and Webba Da Silva,M. (2011) Topological characterization of nucleic acid G-quadruplexes by UV absorption and circular dichroism. *Angew. Chem. Int. Ed. Engl.*, **50**, 10645–10648.
60. Wang,Z., Li,M., Chen,W., Hsu,S.D. and Chang,T. (2016) A novel transition pathway of ligand-induced topological conversion from hybrid forms to parallel forms of human telomeric G-quadruplexes. *Nucleic Acids Res.*, **44**, 3958–3968.
61. Trizna,L., Janovec,L., Halaganová,A. and Víglaský,V. (2021) Rhodamine 6g-ligand influencing G-quadruplex stability and topology. *Int. J. Mol. Sci.*, **22**, 1–15.
62. Demkovičová,E., Bauer,Ľ., Krafčíková,P., Tlučková,K., Tóthova,P., Halaganová,A., Valušová,E. and Víglaský,V. (2017) Telomeric G-quadruplexes: from human to tetrahymena repeats. *J. Nucleic Acids*, **2017**.
63. Garoff,R.A., Litzinger,E.A., Connor,R.E., Fishman,I. and Armitage,B.A. (2002) Helical aggregation of cyanine dyes on DNA templates: effect of dye structure on formation of homo- and heteroaggregates. *Langmuir*, **18**, 6330–6337.
64. Platella,C., Riccardi,C., Montesarchio,D., Roviello,G.N. and Musumeci,D. (2017) G-quadruplex-based aptamers against protein targets in therapy and diagnostics. *Biochim. Biophys. Acta Gen. Subj.*, **1861**, 1429–1447.
65. Musumeci,D., Platella,C., Riccardi,C., Moccia,F. and Montesarchio,D. (2017) Fluorescence sensing using DNA aptamers in cancer research and clinical diagnostics. *Cancers.*, **9**, 174.